Water-induced formation of cobalt-support compounds under simulated high conversion Fischer-Tropsch environment

Moritz Wolf,[†,1] Emma K. Gibson,[‡,§] Ezra J. Olivier,[⊥] Jan. H. Neethling,[⊥] C. Richard A. Catlow,[‡,∥] Nico Fischer,[†] and Michael Claeys[,†]*

[†]Catalysis Institute and c*change (DST-NRF Centre of Excellence in Catalysis), Department of Chemical Engineering, University of Cape Town, Private Bag X3, Rondebosch 7701, South Africa.

[‡]UK Catalysis Hub, Research Complex at Harwell, RAL, Oxford, OX11 0FA, United Kingdom.

[§]School of Chemistry, University of Glasgow, Glasgow, G12 8QQ, United Kingdom.

[⊥]Centre for High Resolution Transmission Electron Microscopy, Physics Department, Nelson Mandela University, PO Box 77000, Port Elizabeth, 6031, South Africa.

[∥]Department of Chemistry, University College London, London, WC1H 0AJ, United Kingdom

ABSTRACT

Herein we present a comparative study on the water-induced formation of metal-support compounds from metallic cobalt in a simulated high conversion Fischer-Tropsch environment. Literature on the deactivation of supported cobalt catalysts *via* oxidation to cobalt(II) oxide or cobalt-support compounds is contradictory due to a lack of use in suitable model catalysts and insufficient direct characterization of the metallic cobalt phase under reaction conditions. The particular carrier materials stabilize the active cobalt nanoparticles, but also dictate the likelihood of the formation of non-active cobalt-support compounds. In this study, well-defined cobalt nanoparticles of 5 nm were deposited on alumina, silica, and three titania carriers. The stability of the reduced nanoparticles against water-rich H_2 atmospheres during exposure to simulated high Fischer-Tropsch conversion levels was monitored in an *in situ* magnetometer. Co/SiO_2 was shown to be the most stable model catalyst, while various Co/TiO_2 model systems readily formed large amounts of cobalt-support compounds at low ratios of the Fischer-Tropsch product H_2O to reactant H_2 or even during the preceding reduction of the oxidic precursor. Co/Al_2O_3 displayed a surprisingly high stability at industrially relevant conditions, in contradiction to thermodynamic predictions. However, cobalt aluminate forms at increased concentrations of water. The existence of hard-to-reduce metal-support compounds in the spent catalysts was confirmed and characterized

[1] Present address: Institute of Chemical Reaction Engineering, University of Erlangen-Nuremberg, 91058 Erlangen, Germany

by means of X-ray absorption near edge structure spectroscopy and high-resolution scanning transmission electron microscopy of the exposed and passivated model catalysts.

KEYWORDS

Metal-support interaction, metal-support compound, cobalt catalyst, in situ magnetic measurement, oxidation, water, XANES, HRSTEM, EELS, Fischer-Tropsch

INTRODUCTION

The Fischer-Tropsch (FT) process describes the conversion of synthesis gas to hydrocarbons. However, the actual main product is H_2O as one molecule is formed for every carbon atom in the paraffinic and olefinic product spectrum (Equation 1). Paradoxically, the *in situ* formed mildly oxidizing molecule is reported to be the major cause for intrinsic catalyst deactivation in the Co-based Fischer-Tropsch synthesis (FTS). Hydrothermal sintering resulting in a loss of active surface area[1–4] or oxidation of FT active metallic Co to inactive oxidic phases may be at play.[5–8] An Ostwald ripening sintering mechanism on Al_2O_3 hydroxylated by H_2O has recently been suggested by Claeys *et al.*, which requires a combination of high concentrations of H_2O and CO in order to facilitate a CO-assisted transport of Co subcarbonyl species over the hydroxylated Al_2O_3 surface.[4] The high mobility of different Co subcarbonyl species has recently been demonstrated in a theoretical study applying density functional theory (DFT),[9] which supports the hypothesized sintering mechanism for Al_2O_3-supported Co catalysts. Aside from a participation of the support, the surface oxidation/reduction cycle upon CO cleavage and the formation of H_2O, which represents a basic step in the FT mechanism, has been hypothesized to result in a continuous structural re-arrangement.[3] This local oxidation and reduction of the Co surface consequentially leads to a higher mobility of the Co atoms facilitating crystallite growth *via* particle coalescence.[3]

$$2H_2 + CO \rightarrow (-CH_2-) + H_2O \qquad (1)$$

Deactivation *via* H_2O-induced oxidation to CoO and cobalt-support compounds[5] is discussed robustly in literature.[6–8,10] The discrepancies can mostly be ascribed to a variety of applied conditions, sizes of cobalt particles ranging from the lower nanometer range up to micrometers,[11] as well as the utilization of various support materials. Inadequate characterization techniques that cannot monitor the metallic phase directly contribute to the confusion.[11] Recent *in situ* studies have elucidated the H_2O-induced oxidation of Co to CoO.[12–14] Oxidation of Co *via* H_2O splitting forming H_2 and CoO has been identified to be kinetically hindered[12,14] due to the high stability of the intermediate hydroxyl groups on the Co surface.[15–17] The direct oxidation of Co to CoO by H_2O was previously identified to be hindered even in the absence of H_2.[18] In contrast, H_2O-induced oxidation *via* CO-derived oxygen is intrinsically embedded in the FT mechanism. The facile dissociation of CO on the Co surface provides an increased concentration of adsorbed oxygen atoms.[5,19] The regeneration of the Co surface *via* removal of said atoms by activated H_2 forming the product H_2O may be hindered under high conversion levels due to the associated high concentration of H_2O.[5,19] Such a deactivation mechanism has been reported to result in rapid

oxidation for sufficiently high partial pressures of CO and is the dominating oxidation process of Co during the FTS.[14]

From a thermodynamic point of view, oxidation of Co to CoO by H_2O is feasible if the energetic state of CoO plus H_2 is favored over metallic Co plus H_2O. For bulk fcc-Co, a partial pressure ratio of H_2O to H_2 (p_{H2O}/p_{H2}) exceeding 128 is required to initiate this oxidation reaction.[10,19] However, commercial CO conversion levels are limited as to not exceed a threshold partial pressure of H_2O[5] and are typically in the range of 60-80% corresponding to p_{H2O}/p_{H2} ratios of 0.75-2. It has to be noted that the partial pressure of H_2O is one of the major reasons for a limited upper conversion in commercial processes[20] as even such relatively low ratios may be sufficiently high to oxidize nano-sized Co.[5] A size dependent oxidation behavior to CoO has been demonstrated for such widely applied Co nanoparticles,[12–14,21] which is facilitated by the drastically increased relative contribution of the surface energy to the overall energy in the case of nanoparticles,[19] *i.e.* nanoparticles experience a pronounced drive for the minimization of their surface energy *via* oxidation to CoO, which has a lower surface energy than Co.[19] A thermodynamic assessment of this size dependency by van Steen *et al.* resulted in the prediction of a critical diameter for oxidation of 4.4 nm for fcc-Co at commercially relevant conditions (p_{H2O}/p_{H2} = 1.5; T = 220 °C),[19] but did not take the highly relevant partial pressure of CO into account.

Another deactivation pathway *via* oxidation of Co is the formation of cobalt-support compounds such as cobalt aluminate or cobalt silicate in a solid-state reaction with commonly used metal oxide carriers. The physicochemical properties of the carriers dictate the likelihood of the formation of such cobalt-support compounds, but also beneficially stabilizes the active Co phase. The formation of metal-support compounds (MSCs) is typically associated with high temperatures and/or the exposure to high concentrations of H_2O.[10,12,13,22] Thermodynamically and for bulk hcp-Co, MSCs are expected to form on various supports at significantly lower p_{H2O}/p_{H2} ratios than those required for the formation of CoO (Figure 1a). For the selected support phases and at 220 °C, a typical temperature for the Co-based FTS, cobalt aluminates are predicted to form at low ratios below 0.1, while titanates are less likely to form. The formation of silicates can be expected to require ratios above 10, which exceeds industrially relevant conversion levels. However, the widely applied amorphous SiO_2 may display a different behavior than quartz, the assumed SiO_2 phase in our calculations.

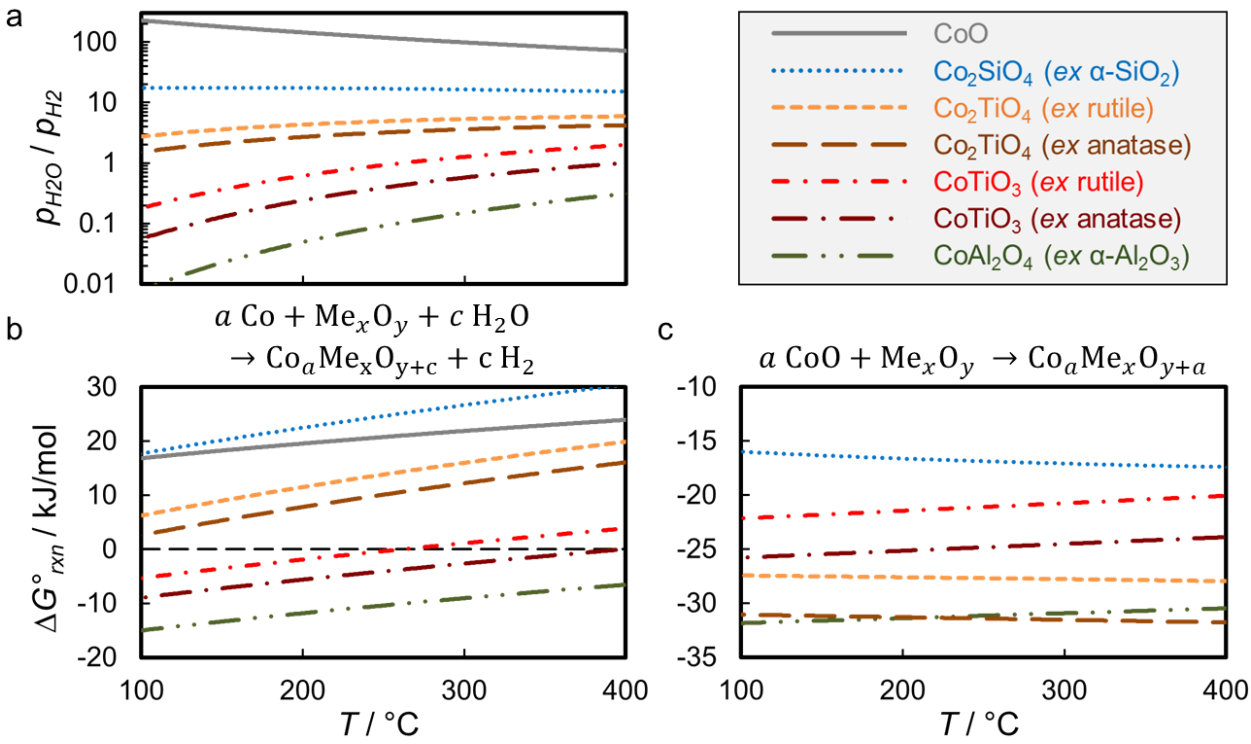

Figure 1. (a) Thermodynamic equilibria and (b) Gibbs free energies for selected oxidation reactions of bulk hcp-Co by gaseous H_2O, as well as (c) Gibbs free energies of selected solid-state reactions of CoO with common metal oxide carriers calculated with thermodynamic data from Knacke *et al.*[23] The thermodynamic equilibria for the oxidation of hcp-Co to CoO, Co_2SiO_4, Co titanates *ex* rutile, and $CoAl_2O_4$ were adapted from Wolf *et al.*[12]

The Gibbs free energies of the solid-state reactions of the metallic Co phase, H_2O, and the particular carrier material describe the feasibility for a CO conversion level of 66.67% (Figure 1b), which corresponds to a 1:1 ratio of H_2O to H_2 (p_{H2O}/p_{H2} = 1) according to the generalized FT reaction (Equation 1). The formation of cobalt aluminates has previously been hypothesized to be kinetically hindered,[10] while the negative Gibbs free energy for this particular reaction strongly suggests a spontaneous reaction. Other crystal structures of Al_2O_3 are reported to show a higher tendency towards the formation of aluminates than the here considered γ-Al_2O_3.[24,25] The high Gibbs free energies for the oxidation of Co by H_2O forming CoO and Co_2SiO_4 indicate a low feasibility of formation, while the negative values for $CoTiO_3$ at lower temperatures suggest the formation of cobalt-support compounds for anatase and for rutile, with the latter being less likely. The formation of cobalt-support compounds from CoO is thermodynamically feasible for all supports in the considered systems (Figure 1c). Besides a strong dependency on the metal oxide and the crystal structure, the morphology of the supports such as porosity and the reducibility can be expected to alter the likelihood of the formation of MSCs.

Tsakoumis *et al.* recently observed the formation of cobalt aluminates in an impregnated Co/Re/γ-Al_2O_3 catalyst at approximated CO conversion levels of 60-65% by monitoring the cobaltous phases during FTS *via in situ* X-ray absorption near edge structure (XANES).[13] When all phases were in equilibrium, the concentration of CoO was marginally increased when compared to the reduced catalyst, while 8% of $CoAl_2O_4$ were identified.[13] Based on the hypothesised size dependent re-oxidation of Co to CoO,[19] a mechanism for the formation of cobalt aluminate *via* a multilayer re-oxidation of Co crystallites below 5.3 nm to CoO was proposed, which is followed

by spreading of the nanoparticle over the support and the subsequent formation of the MSC.[13] Such a formation of aluminates from CoO, which either originates from re-oxidation or is present as un-reduced CoO after reduction representing a spectator species, but slowly diffuses into the support in a kinetically hindered solid-state reaction upon exposure to high concentrations of H_2O, has previously been hypothesized.[10,26]

In the present study, separately synthesized Co_3O_4 nanoparticles were deposited on commonly applied metal oxide support materials. The resulting physical mixtures represent the parent catalysts and no further treatment such as calcination is required. Thus, this model catalyst system, in combination with mild reduction temperatures in H_2, is expected to prevent the formation of MSCs prior to reduction and/or exposure to H_2O-rich environments, *i.e.* during catalyst preparation or activation. In addition, the absence of CO allows for the almost exclusive characterization of the formation of cobalt-support compounds as the oxidation of Co to CoO by H_2O is kinetically hindered.[12,14] Indirect oxidation by H_2O, that is the hindering of surface regeneration *via* O* removal following CO dissociation on the Co surface and resulting in the formation of CoO, is avoided by the absence of CO.[12,14] Lastly, the magnetic *in situ* characterization of the model catalysts exposed to H_2O-rich environment provides a direct quantitative information on the amount of metallic Co present, *i.e.* only monitors the potential formation of MSCs from the metallic phase. The formation of MSCs was tested at various ratios of FT product H_2O to reactant H_2 and compared to the stability of Co nanoparticles in a similar model catalyst system utilizing SiO_2 Stöber spheres as support material presented elsewhere.[12] A subsequent complementary characterization of the exposed and passivated catalysts by means of XANES spectroscopy and high-resolution scanning transmission electron microscopy (HRSTEM) allows for the analysis of formed oxidic cobalt species.

METHODS AND EXPERIMENTAL DETAILS

Materials. Acetone (≥99.3% purity), aqueous ammonium hydroxide solution (min. 25 wt.%), diethyl ether (≥99.0% purity), and ethanol (≥99.9% purity) were purchased from Kimix (South Africa), benzyl alcohol (ACS reagent, ≥99.0% purity), cobalt(II) acetate tetrahydrate (reagent grade), silica gel (grade 923, 100-200 mesh), anatase-TiO_2, and rutile-TiO_2 were purchased from Sigma-Aldrich, P25-TiO_2 was supplied from Degussa (Germany, now Evonik), and Puralox-Al_2O_3 from Sasol Germany. All chemicals were used as received, while the metal oxide supports were dried at 120 °C in air for >24 h prior to use.

Synthesis of Co_3O_4 nanoparticles. Co_3O_4 nanoparticles were synthesized *via* a surfactant-free, nonaqueous heat treatment of dissolved cobalt acetate tetrahydrate in benzyl alcohol in the presence of ammonium hydroxide.[12,14,27,28] In short, an amount of 1600 mg of cobalt acetate tetrahydrate was dissolved in 70 mL benzyl alcohol under magnetic stirring (500 rpm) in a round bottom flask. After 2 h of stirring, 70 mL of a 25 wt.% $NH_4OH_{(aq)}$ solution were added dropwise to the pink to purple solution forming a brown emulsion. Once the addition of $NH_4OH_{(aq)}$ was completed, the flask was transferred to a preheated oil bath of a rotary evaporator set-up and heated for a total of 3 h at an overall pressure of 900 mbar while the flask was rotated at 180 rpm. Air was bubbled through the reaction emulsion during the synthesis in the rotary evaporator to provide adequate mixing.[27]

Anchoring of the nanoparticles on the supports. Co_3O_4 nanoparticles were dispersed in ethanol in an ultrasonic bath until the nanoparticles were in dispersion. The particular amount of Puralox-Al_2O_3, P25-TiO_2, rutile-TiO_2, or anatase-TiO_2 support material targeting a loading of 0.5 wt.%

metallic Co were sonicated in ethanol under mechanical stirring *via* an overhead stirrer. After 4 h, the dispersion of Co_3O_4 nanoparticles in ethanol was added dropwise under continuous ultrasonication and mechanical stirring. After another 4 h, the dispersion was transferred to a rotary evaporator and further mixed for 1 h at 240 rpm and 80 °C. Lastly, ethanol was evaporated from the parent catalyst at 462 mbar.[12,14] A very low catalyst loading was chosen for these model catalysts so as to minimize effects of sintering, which may cloud observations, *i.e.* to isolate the formation of MSCs from other deactivation mechanisms.

Methodology of the *in situ* magnetometer. An *in situ* magnetometer, which is based on the Weiss extraction method and was developed at the University of Cape Town in cooperation with Sasol, was utilized for the *in situ* characterization of the supported cobalt-based model catalysts (Figures S6-S7).[4,12,21,29] The ½" stainless steel fixed bed reactor is heated *via* infrared heaters and temperatures of up to 900 °C can be realized. Reactor pressures exceeding 50 bar can be applied. A resistance temperature detector (Pt100) placed inside the catalyst bed measures the temperature allowing for an accurate control of the reactor temperature (Figure S8). In this set-up, a current-controlled electromagnet provides external magnetic field strengths of up to ±2 T (20 kOe).

In the present study, the low Néel temperatures of oxidic cobalt species and the high Curie temperature of metallic Co lead to the latter being the only species displaying magnetic susceptibility and remnant magnetization (M_{rem}) upon removal of an external magnetic field (see supporting information and Table S1 for an extended introduction to magnetism of cobaltous species). Thus, the measured magnetization at maximum external field strength is directly proportional to the amount of metallic Co in the reactor and approximates the saturation magnetization (M_S). As the amount of loaded Co in the reactor is known, the obtained saturation magnetization of the sample can be compared to the saturation magnetization of 100 mg metallic bulk Co of a calibration curve ($M_{S,cal}$) to obtain a degree of reduction (*DOR*) for the metallic Co phase (Equation 2).The remnant magnetization is herein obtained by interpolation of four measured magnetization readings between 0.03 and -0.01 T to 0 T upon removal of the external magnetic field.[30]

Ferromagnetic materials behave superparamagnetic below a certain material specific crystallite size, *i.e.* these materials cannot retain a remnant magnetization upon removal of an external field.[31] The exact critical size for superparamagnetism in metallic Co is still under debate[2,32] (approximately 15-20 nm for fcc-Co at room temperature).[30,33,34] The mass fraction of material with "large crystallite sizes" displaying remnant magnetization (γ) can be calculated from the saturation magnetization (M_S) and the remnant magnetization (M_{rem}; Equation 3).[30] The γ value describes the relative mass of ferromagnetic domains larger than the critical diameter for superparamagnetism. Hence, an increase in γ can be interpreted as an increased mean crystallite size and/or a decreased overall fraction of smaller crystallites in the metallic phase.

$$DOR = \frac{M_S(T)}{M_{S,cal}(T)} \cdot \frac{100\ \text{mg}}{m_{Cat} \cdot x_{Co}} \cdot 100\% \quad (2)$$

$$\gamma = \frac{2 \cdot M_{\text{rem}}(T)}{M_S(T)} \cdot 100\% \quad (3)$$

Where m_{Cat} is the amount of catalyst loaded in mg and x_{Co} is the Co mass loading.

The size distribution of superparamagnetic metallic Co crystallites can be obtained by a combination of size-specific Langevin equations on the measurement of the magnetization as a function of the external field strength.[30] However, relatively high γ values of above 10 wt.%

preclude a reasonable application of the Langevin equation as the broadening of the sigmoid-type curve resulting in a hysteresis behavior cannot be described by the Langevin equation. For this reason, the Langevin equation was applied on the anhysteretic magnetization curve only and this was modelled *via* the Jiles-Atherton method[35,36] (see supporting information and Figures S1-S2 for further details). This processing of the raw data allows for the calculation of the size distribution of the magnetic Co domains displaying superparamagnetic behavior only, *i.e*. magnetic domains/crystallites below the threshold size for superparamagnetism excluding larger ones.[14]

Experimental procedure in the *in situ* magnetometer. A total amount of 2003.6 mg of the oxidic parent catalyst was placed in the reactor and reduced in a 50% H_2 in Ar atmosphere at a gas hourly space velocity (GHSV) of 6000 mL/($g_{catalyst}$·h) and a heating rate of 1 °C/min. The reduction temperature was increased stepwise from 300 to 340 to 360 °C with a holding time of 8 h each to minimize thermal strain with possibly accompanied sintering during reduction.[12] The onset temperature of the reduction was defined as the first change of sign in the first derivative of the sample magnetization (obtained at 2 T) as a function of temperature to positive values. After cool-down to 220 °C, the flow rates of H_2 and Ar were adjusted to obtain a GHSV of 369 mL_{H2}/($g_{catalyst}$·h) and 2126 mL_{Ar}/($g_{catalyst}$·h), respectively, and kept constant throughout all consecutive steps. Subsequently, the partial pressure of H_2O was incrementally increased to simulate a range of FT conversion levels in order to initiate water-induced oxidation of Co to MSCs (Figure 2), while only minor oxidation of Co to CoO can be expected due to a kinetically hindered direct oxidation by H_2O.[14] The amount of co-fed H_2O was regulated *via* an HPLC pump and mixed with the inlet gas stream in a vaporizer, while the absolute pressure was increased accordingly (Table 1). All levels were monitored for at least two hours before applying the subsequent conditions. The reversibility of a potential loss in magnetization representing oxidation was tested in a last step in a dry H_2/Ar atmosphere upon removing H_2O from the feed stream, while the overall pressure was kept constant for up to 2 h before decreasing to atmospheric pressure. To distinguish between reducible cobalt oxide and possibly formed hard-to-reduce cobalt-support compounds, the samples were re-reduced while heating at 1 °C/min to the maximum reduction temperature of 360 °C with a holding time of 0.5 h (Figure 2). After cool-down to room temperature, the catalysts were passivated in 1% O_2/N_2 at a GHSV of 1500 mL/($g_{catalyst}$·h) for several hours[37] to protect potentially accessible metallic Co surface from violent oxidation upon exposure to air by forming a thin layer of CoO (Figure 2). Lastly, the spent and passivated samples were collected for additional post-run *ex situ* analysis. The sample magnetization at high external field strengths and the remnant magnetization were measured every 6 min ("quick test") and a 65 point *M-H* measurement was taken during the last 30 min of each step (Figure S9).

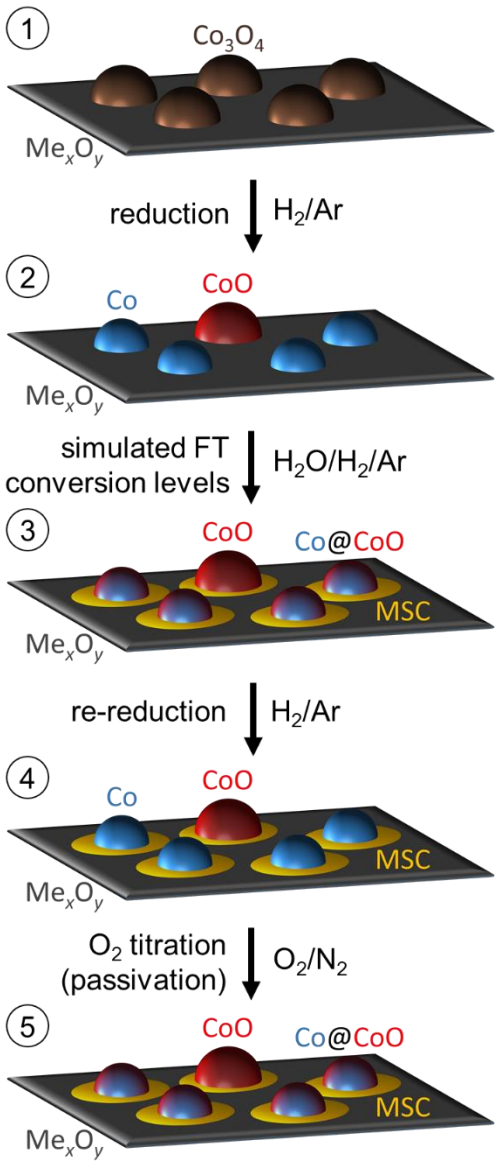

Figure 2. Graphical depiction of the expected cobaltous phases during the experimental procedure in the *in situ* magnetometer: 1. as prepared parent Co_3O_4/Me_xO_y model catalyst, 2. metallic Co/Me_xO_y catalyst after reduction with a fraction of not fully reduced CoO nanoparticles, 3. exposed catalyst after simulating high Fischer-Tropsch conversion levels in water-rich atmospheres potentially inducing the formation of metal-support compounds and, to a minor extent, surface oxidation of Co nanoparticles, 4. re-reduced model catalyst after hydrogen treatment at moderate temperatures in order to reverse partial oxidation of Co to CoO, and 5. passivated catalysts with a thin CoO oxidation layer on accessible Co nanoparticles protecting the pyrophoric metallic core from violent oxidation by air.

Table 1. Applied conditions for the incremental increase of the simulated Fischer-Tropsch conversion levels during in situ magnetic measurements upon reduction.

H_2O level	p_{H2O} / bar	p_{H2} / bar	p_{Ar} / bar	p_{H2O}/p_{H2}	$X_{CO,sim}$ / %	p / bar
1	0.02	0.15	0.85	0.15	25.93	1.02
2	0.22	0.15	0.85	1.50	77.78	1.22
3	0.73	0.15	0.85	5.00	92.11	1.73
4	1.45	0.15	0.85	10.00	95.89	2.45
5	2.90	0.15	0.85	20.00	97.90	3.90
6	4.35	0.15	0.85	30.00	98.59	5.35
7	5.80	0.15	0.85	40.00	98.94	6.80
8	7.25	0.15	0.85	50.00	99.15	8.25
-	-	0.15	0.85	0.00	-	1.00

X-ray absorption spectroscopy (XAS). The cobalt oxide standards CoO and Co_3O_4,[27] as well as the standards for the cobalt-support compounds cobalt aluminate[38,39] and cobalt titanate[39] were synthesized in benzyl alcohol according to reported sol-gel methods. Cobalt silicate was prepared in a hydrothermal synthesis described in literature.[40] XANES spectra were obtained at the Co K-edge at beamline B18 (beamtime number sp15151) of the Diamond Light Source[41] in Harwell, United Kingdom. Measurements of the standards were performed in transmission mode (3 repetitions), while the exposed and passivated model catalysts were measured in fluorescence mode (12 repetitions). All spectra were acquired with a Co foil placed before the reference detector. The raw data was processed in Athena of the open-source software package Demeter,[42] which is based on the IFEFFIT library.[43] Linear combination fitting (LCF) of the samples with the particular standards was conducted in the first derivative of the normalized XANES spectra in the energy range from -20 to 50 eV relative to the edge using Athena. Additional extended X-ray adsorption fine structure (EXAFS) spectra were modeled in Artemis, which is also part of the software package Demeter.[42]

Transmission electron microscopy (TEM). The bare support materials were dispersed in acetone *via* ultrasonication for 5 min and deposited onto carbon-coated copper grids. The as prepared Co_3O_4 nanoparticles were dispersed in ethanol for 30 min prior to deposition. TEM analysis was conducted using a Tecnai F20 microscope (Philips) equipped with a field emission gun and operated at 200 kV (Gatan). Imaging was done with a US4000 4kX4k CCD camera (Gatan). The exposed and passivated model catalysts were dispersed in acetone *via* ultrasonication for 5 min and deposited onto Quantifoil holey carbon film grids. Analysis of the samples *via* high-resolution scanning transmission electron microscopy (HRSTEM) was conducted at atomic resolution using a double spherical aberration corrected JEM-ARM200F microscope (JEOL). The samples were studied with bright field and dark field imaging. A GIF electron spectrometer with dual electron energy loss spectrometry (EELS) imaging capabilities and an XMax 100 TLE high collection angle, ultra-sensitive detector (Oxford Instruments) was applied for analysis by means of energy-dispersive spectrometry.

X-ray diffraction (XRD). XRD was conducted at 35 kV and 40 mA in a Bruker D8 Advance, equipped with a Co source ($\lambda_{K\alpha 1}$ = 1.78897 Å) and a position sensitive detector (LYNXEYE XE, Bruker AXS) from 20-120° at a step size of 0.025° with an exposure time of 1 s per step. The

diffraction patterns were compared to reference patterns of the Powder Diffraction File of the International Centre for Diffraction Data (PDF-2 Release 2008; Co_3O_4: 00-043-1003, anatase-TiO_2: 01-086-1157, rutile-TiO_2: 01-089-0554, γ-Al_2O_3: 00-025-0251, γ-AlOOH: 01-072-0359).[44] The crystallite size and weight fraction of identified phases were determined by Rietveld refinement of the XRD patterns (TOPAS 5, Bruker AXS).[45] Diffraction line broadening analysis *via* the Scherrer equation[46] with correction for the instrumental line broadening and a shape factor of 0.9 was applied as a second method[47] to gain information on the crystallite size of the unsupported Co_3O_4 nanoparticles using the 311 reflection.

BET surface area and BJH pore volume. Analysis of the surface area and the pore volume of the supports was conducted in a Micromeritics TriStar II 3020 with N_2 as analysis adsorptive and a degassing temperature of 200 °C. Errors for obtained BET surface areas represent the uncertainty of measurement, which depends on the mass of loaded sample, the correlation coefficient of the fit to the Brunauer-Emmett-Teller equation, and the blank error of the physisorption measurements.

Inductively coupled plasma optical emission spectrometry (ICP-OES). The samples were pre-treated overnight in a 4:1 molar ratio of aqua regia:HF. Subsequently, the sample was heated at a heating rate of 6.4 °C min^{-1} to 180 °C for 40 min during microwave digestion (1600 W) in order to obtain the cobalt loadings or metal concentrations *via* elemental analysis in a Varian ICP-OES 730.

RESULTS AND DISCUSSION

Characterization of the parent catalysts. The bare supports were characterized by means of XRD (Figures S10-S11) to identify the phase compositions, as well as by physisorption according to the BET and BJH methods (Figures S12-S13) and TEM (Figure S14) to obtain information on the morphology of the support materials (Table 2). The BET surface areas can also be considered as a representation of the surface areas of the supported catalyst as the low targeted Co-loading of 0.5 wt.% can be expected to not impact on these. Stöber spheres are amorphous, while the Al_2O_3 Puralox (Sasol), the mixed-phase TiO_2 P25 (Degussa, now Evonik), and single-phase anatase and rutile (TiO_2; Sigma-Aldrich) are crystalline with P25 consisting of 81 wt.% anatase and 19 wt.% rutile. No crystalline impurities were detected in the anatase and rutile supports by means of XRD, while Puralox required a calcination at 500 °C in order to transform impurities of aluminum oxide hydroxide (boehmite, AlOOH) into Al_2O_3. XRD analysis only allows for the identification of γ-Al_2O_3 in the Puralox carrier after calcination, but other Al_2O_3 phases may be present as well.

Table 2. Characterization of the supports and the parent catalysts.

Support	Metal oxide	Crystal structure(s)	BET surface area / m^2/g	BJH pore volume / cm^3/g	BJH pore size / Å	Co in parent catalyst / wt.%
Puralox	Al_2O_3	γ-Al_2O_3	151 ± 0.6	0.46	96	0.42
Stöber	SiO_2	Amorphous	19 ± 0.1	0.08	148	0.43
P25	TiO_2	4:1 anatase:rutile	49 ± 0.2	0.18	147	0.41
Anatase	TiO_2	Anatase	98 ± 0.5	0.26	85	0.42
Rutile	TiO_2	Rutile	27 ± 0.1	0.11	160	0.40

The synthesized Co_3O_4 nanoparticles were previously analyzed (Figure S15) resulting in a volume mean crystallite size of 5.0 nm, 5.5 nm, or 3.8 ± 0.7 nm according to Scherrer equation, Rietveld refinement, and TEM analysis, respectively.[12] Elemental analysis of the parent catalysts after deposition of the separately synthesized Co_3O_4 crystallites *via* ICP-OES resulted in actual Co loadings between 0.40 and 0.43 wt.% (Table 2). The low concentration of Co prohibits analysis of the supported cobaltous phase in the catalysts by means of conventional XRD after deposition of the nanoparticles on the support materials.

***In situ* magnetic characterization during reduction.** The model catalysts (2003.6 mg) were loaded in the fixed bed reactor of the *in situ* magnetometer and reduced in 50% H_2/Ar at stepwise increasing temperatures to minimize thermal strain and possibly accompanied sintering. The reduction behavior of the catalysts is strongly affected by the support material (Figure 3; see detailed discussion and Figures S3-S5 in the supporting information). The DOR of the Co_3O_4 nanoparticles to metallic Co on the various supports after reduction decreases in the order rutile-TiO_2 > SiO_2 > P25-TiO_2 > Al_2O_3 > anatase-TiO_2 resulting in final values ranging from 35-70%. The latter catalyst demonstrates a particularly intriguing reduction behavior as the magnetization initially increases due to the reduction of cobalt oxide to metallic Co, but subsequently decreases sharply at temperatures exceeding 280 °C. Hence, previously reduced Co is transformed into a non-magnetic phase even though the catalyst is exposed to a reducing 50% H_2/Ar atmosphere at a high GHSV, *i.e.* the concentration of formed H_2O during reduction can be expected to be rather low. Almost half of the initially formed metallic cobalt phase is transformed within 2 h at 300 °C with a presumably underlying ongoing reduction of unreduced cobalt oxide. The final DOR (in terms of ferromagnetic Co) of 35% is only marginally higher than the DOR of 30% at 280 °C.

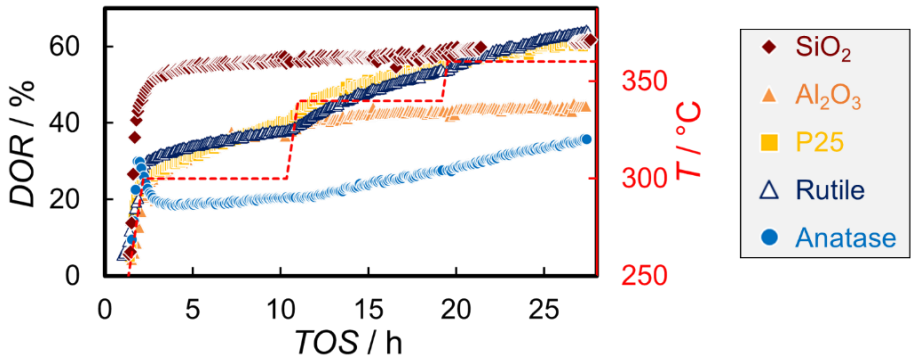

Figure 3. Degree of reduction to metallic cobalt of the model catalysts as a function of time on stream and the temperature (dashed) during reduction in 50% H_2/Ar. The reduction of the Co/SiO_2 model catalyst is adapted from Wolf *et al.*[12]

A partial reduction of the surface of anatase-TiO_2 has been reported for impregnated catalysts containing platinum group metals at 200 °C.[48–52] The reduction takes place in close vicinity of the metal particles, but more isolated surface ions can also be (partially) reduced at increased temperatures. A H* spillover type mechanism[53–56] from the Co to the TiO_2 support has been suggested, which catalyzes the reduction of TiO_2 in Co-based catalysts.[48] In contrast to anatase, no such a partial reduction has been reported for rutile-supported catalysts. This process is presumably accompanied by an increased mobility of Ti ions.[49] Aside from partial (surface) reduction of the anatase support, a H_2O-induced mechanism forming cobalt titanate-type species is supported by literature. Jongsomjit *et al.* co-fed up to 10% H_2O during reduction of a Co/anatase-

TiO_2 catalyst in H_2, which induced a shift of the reduction temperature by 10-20 °C as observed *via* temperature programmed reduction (TPR) indicating pronounced metal-support interaction.[57] Further, a delayed reduction of an anatase-supported Co catalyst was observed *via* TPR when compared to Co on a single-phase rutile support.[58,59] A temperature shift was not observed for a rutile concentration of 19 wt.% in a TiO_2 support,[57] *i.e.* the composition of P25. A beneficial effect of the presence of rutile in a Co-based catalyst with a mixed-phase TiO_2 support is also reported for CO hydrogenation.[57,59] A concentration of at least 3 wt.% of rutile drastically facilitated the reduction process of cobalt oxide species and in turn increased the activity of the catalyst. Further, higher concentrations of the anatase polymorph induced a more pronounced deactivation when comparing the initial activity to the steady-state conditions.[59]

In summary, literature and the present results suggest a phase dependency of the stability of Co on TiO_2 during reduction, which is either originated in the relatively high surface reducibility of anatase-TiO_2[48–52] or in the formation of H_2O oxidizing the metallic Co phase.[57] The latter is predicted by thermodynamics (Figure 1) even though low concentrations of H_2O are expected due to the high GHSV. Either way, the formation of a non-ferromagnetic phase *via* a solid-state reaction of (partially reduced) anatase with metallic Co is expected and observed during reduction of the Co/anatase-TiO_2 catalyst in the present study (Figure 3). Both, oxidation to a cobalt titanate-type species or the formation of a cobalt-titanium alloy are plausible as both phases cannot be magnetized and hence not be detected in the magnetometer at the given conditions.[60–63]

Different trends for the reducibility of supported cobalt oxide on metal oxide carriers have been reported in literature.[64–68] Comparison of the reduction behavior of the Al_2O_3-supported catalysts with the other metal oxide supports reveals a hindered reduction of Co_3O_4 nanoparticles to Co (Figure S4). Strong interaction of cobalt oxide with Al_2O_3 is well accepted in literature.[68] In contrast, Co/TiO_2 catalysts have been reported to have the highest reducibility of cobalt oxide in several comparative studies,[64–67] while the group of Davis reported the best reducibility for SiO_2-supported catalysts.[68,69] However, comparison of the impregnated and calcined catalysts comprising different crystallite sizes and probably different morphologies of Co_3O_4 on the supports is challenging and may be misleading. Further, various conditions during calcination may induce varying metal-support interaction for the different supports prior to reduction.[70] Lastly, reduction promoters potentially contribute to the contradiction and, as demonstrated in the present study for the TiO_2-supported catalysts, the reduction behavior also changes for polymorphism of the support material.

In situ **magnetic characterization during simulated FT conversion.** After reduction, the model catalysts were exposed to H_2O/H_2/Ar atmospheres. The partial pressures of H_2 and Ar were kept constant while the amount of co-fed H_2O was incrementally increased to obtain partial pressure ratios of H_2O to H_2 (p_{H2O}/p_{H2}) of 0.15-50 (Table 1). Such an environment simulates FT conversion levels as CO is absent and hence excludes potential effects from an actual formation of hydrocarbons on the Co surface. These model conditions may induce oxidation of Co to CoO, but the direct oxidation of Co by H_2O (water splitting) has previously been identified to be kinetically hindered[12,14] as OH* groups originating from H_2O dissociation on the Co surface are rather stable.[15–17] In turn, a pronounced oxidation to CoO in a FT environment requires the presence of CO, which is absent in this study, as CO increases the concentration of O* upon adsorption and dissociation on the Co surface.[14] Hence, a rapid and significant decrease in the magnetization can be mostly ascribed to oxidation of ferromagnetic Co to non-ferromagnetic MSCs (Figure 2). The

influence of the supports on the limited oxidation to CoO can be expected to be rather small, *i.e.* only differences in the exposure time of the catalysts to the particular H_2O levels may affect the amount of formed CoO. Comparable Co nanoparticles on carbon spheres were previously exposed to H_2O-rich atmospheres in a similar manner and only lost 4% of the magnetization when compared to the magnetization upon reduction (Figure S16),[14] which can be considered as a baseline case as the formation of MSCs with the carbon support are highly unlikely.

In a previous study,[12] the SiO_2-supported Co nanoparticles have been demonstrated to display a high stability against the formation of cobalt silicate as only 6% of the magnetization after reduction was lost after exposure to p_{H2O}/p_{H2} ratios of 0.15-50 (Figure 4). High p_{H2O}/p_{H2} ratios of ≥20 were required to initiate the oxidation process.[12] In the present study, the magnetization of Co/Al_2O_3 is stable at low p_{H2O}/p_{H2} ratios (Figure 4) even though thermodynamic predictions suggest a formation of cobalt aluminates at very low concentrations of H_2O (Figure 1). A first decrease can be observed at a p_{H2O}/p_{H2} ratio of 5, *i.e.* outside commercially relevant FT conversion levels (p_{H2O}/p_{H2} ≈ 0.75-2). The decrease of the sample magnetization is rather constant below a p_{H2O}/p_{H2} ratio of 30. Hence, the potential formation of MSCs is not a function of the partial pressures unless exposed to high p_{H2O}/p_{H2} ratios. This behavior suggests a kinetically hindered oxidation process, while oxidation of the Co phase apparently exacerbates when exposed to ratios of 40-50. It has to be noted that significantly more metallic Co is transformed than for Co/SiO_2 indicating an enhanced formation of MSCs.

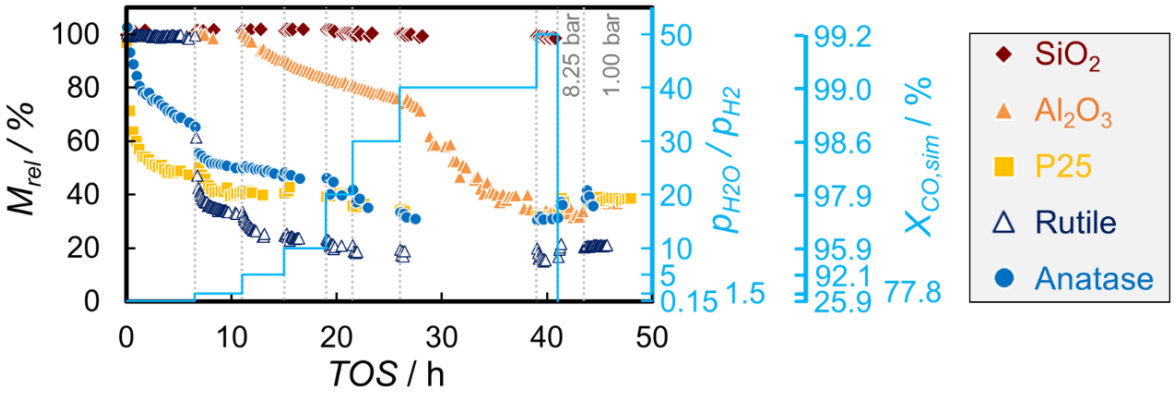

Figure 4. Magnetization at maximum field strength (2 T) relative to the magnetization after reduction of the model catalysts at 220 °C as a function of time on stream with stepwise increase of the ratio of the partial pressures of water to hydrogen (solid) simulating various carbon monoxide conversion levels in the Fischer-Tropsch synthesis. The data of the Co/SiO_2 model catalyst is adapted from Wolf *et al.*[12]

In contrast to the SiO_2- and Al_2O_3-supported Co nanoparticles, the potential formation of MSCs starts at the lowest p_{H2O}/p_{H2} ratio of 0.15 for anatase- and P25-TiO_2, while a ratio of 1.5 is required for rutile-TiO_2 (Figure 4). Further, the oxidation process on these supports is seemingly thermodynamically controlled as the decrease in sample magnetization clearly is a function of p_{H2O}/p_{H2}, *i.e.* the solid-state reaction is accelerated when exposed to increasing amounts of co-fed H_2O. Remarkably, the magnetization of the Co/rutile-TiO_2 catalyst decreases to less than 50% of the magnetization after reduction within 10 min upon exposure to p_{H2O}/p_{H2} = 1.5. These observations confirm a higher stability of Co against H_2O when supported on rutile-TiO_2 as compared to the anatase-TiO_2 or mixed-phase TiO_2 supports. This is in agreement with literature[57]

and the thermodynamic predictions (Figure 1). Even though the presence of rutile-TiO_2 in the P25 support stabilizes the Co nanoparticles during reduction, no significant increase of the stability against oxidation can be observed during exposure to the mildly oxidizing conditions at H_2O level 1 (p_{H2O}/p_{H2} = 0.15). The formation of MSCs in the TiO_2-supported model catalysts is seemingly decelerated at high p_{H2O}/p_{H2} ratios, but this observation may originate from diffusion limitations of the solid-state reaction, *i.e.* unreacted, metallic Co and TiO_2 are not in close vicinity anymore due to the formation of an isolating (oxidic) intermetallic phase. Diffusion of one or both of the reactants is inevitable for further formation of MSCs. Hence, the Co-TiO_2 interface may be considered as saturated with cobalt titanate type species.

In summary, the model catalysts demonstrated a resistance against increasing concentrations of H_2O in the order SiO_2 > Al_2O_3 > rutile-TiO_2 > P25-TiO_2 = anatase-TiO_2 regarding the required ratio of p_{H2O}/p_{H2} for initiation of the decrease in sample magnetization (Figure 4). Neglecting the different exposure times of the model catalysts, the overall decrease in the magnetization is comparable for Co/Al_2O_3, Co/anatase-TiO_2, and Co/P25-TiO_2 and approximately 70% of Co present in the sample after reduction is oxidized. The decrease in the sample magnetization of Co/anatase-TiO_2 is lower than for the other TiO_2-supports, but said catalyst already formed a non-ferromagnetic cobaltous species during the reduction (Figure 3). Hence, direct comparison is misleading. Over 80% of the initially reduced Co on rutile-TiO_2 oxidizes during exposure to H_2O levels 1-8, therefore representing the most strongly oxidized model catalyst.

All catalysts recover a small fraction of the lost magnetization (<5%) when H_2O is removed from the feed stream (Figure 4). Reversible oxidation can mostly be ascribed to re-reduction of CoO to metallic Co.[12,14] MSCs typically require reduction temperatures exceeding 220 °C significantly.[70–72] Hence, the low reversibility at 220 °C confirms the expected limited formation of CoO due to kinetically hindered oxidation of Co by H_2O to CoO.[14] It has to be noted that a potential formation of MSCs *via* CoO as a fleeting species is regarded as negligible. The formation of CoO *via* the kinetically hindered direct oxidation of Co by H_2O is expected to be initiated at similar partial pressure ratios of H_2O/H_2 for all applied support materials.[12,14] A subsequent solid-state reaction of CoO and the particular support would be favourable according to thermodynamic predictions for all studied metal oxide carriers (Figure 1c). However, the decrease in magnetization observed during exposure of the model catalysts to the various p_{H2O}/p_{H2} ratios is dependent on the support material (Figure 4). Thus, a significant contribution of a CoO mediated formation of MSCs can be ruled out in the present study.

The sample magnetization was measured as a function of the external field strength after reduction, at the end of each H_2O level, after removing H_2O from the feed stream, and after re-reduction. Hysteresis behavior was obtained in all samples (for examples see Figure S2) and the analyses thereof allow for the calculation of the size distribution of the smaller superparamagnetic Co nanoparticles *via* a combined application of the Jiles-Atherton method[35,36] and the Langevin equation.[30] Note that the obtained average size and size distribution exclude the larger Co crystallites displaying normal ferromagnetic behavior, *i.e.* displaying remnant magnetization upon removal of an external magnetic field. Further, the calculation of γ, the weight fraction of Co displaying remnant magnetization, provides a qualitative indication of size changes in the metallic Co phase as it describes the fraction of Co nanoparticles larger than the threshold size for superparamagnetic behavior. A decrease in the superparamagnetic Co crystallite size ($d_{V,S}$) may indicate partial oxidation of the Co phase, that is either surface oxidation to CoO, oxidation *via*

solid-state reaction with the support at the Co-support interface, or a combination of both. Besides at the initial interface, MSCs may be formed at the surface of the crystallites if either mobile support species allow for creeping onto the Co surface or Co atoms diffuse onto the surface of the support. All suggested mechanisms can be expected to be sensitive to the accessible surface area of Co and hence are size dependent.

Only little oxidation is observed for Co/SiO_2 during exposure to the various H_2O levels (Figure 4), which does not alter the fraction of Co displaying remnant magnetization and the size of the superparamagnetic Co crystallites (Figure 5).[12] In contrast, the γ value of the P25- and rutile-supported catalysts decrease during exposure to the various H_2O levels (Figure 5a). The decrease in γ is more pronounced when the sample magnetization drops by approximately 70% upon exposure of the single-phase rutile-supported Co crystallites to a p_{H2O}/p_{H2} ratio of 1.5, which strongly suggests a correlation between the decrease in γ and oxidation of Co to MSCs. In contrast, the γ value of Co/anatase increases upon first exposure to H_2O-rich atmospheres when compared to the fraction after reduction. A subsequent decrease during exposure to increased ratios of p_{H2O}/p_{H2} suggests a preferential oxidation of smaller, superparamagnetic Co crystallites at lower p_{H2O}/p_{H2} ratios, while larger ones are (partially) oxidized at ratios exceeding 10. The volume-mean size decreases on the TiO_2-supported catalysts as soon as oxidation of Co by H_2O is detected (Figure 5b). This observation, in combination with a decreasing γ value and a loss in magnetization for rutile- and P25-supported Co, indicates a pronounced loss of Co crystallites larger than the threshold size for superparamagnetism when compared to smaller ones, *i.e.* a size dependent phase change from metallic Co to most likely cobalt titanate. This partial oxidation of the crystallites decreases the size into the superparamagnetic regime. At the same time, superparamagnetic crystallites are partially oxidized resulting in a decrease in both, the γ value and $d_{V,S}$. These two processes are identified separately for the Co/anatase catalyst at H_2O level 1. The mean crystallite size of superparamagnetic Co decreases, while the γ value increases (Figure 5a). Hence, oxidation of the larger Co crystallites on anatase requires an increased p_{H2O}/p_{H2} ratio when compared to the smaller ones.

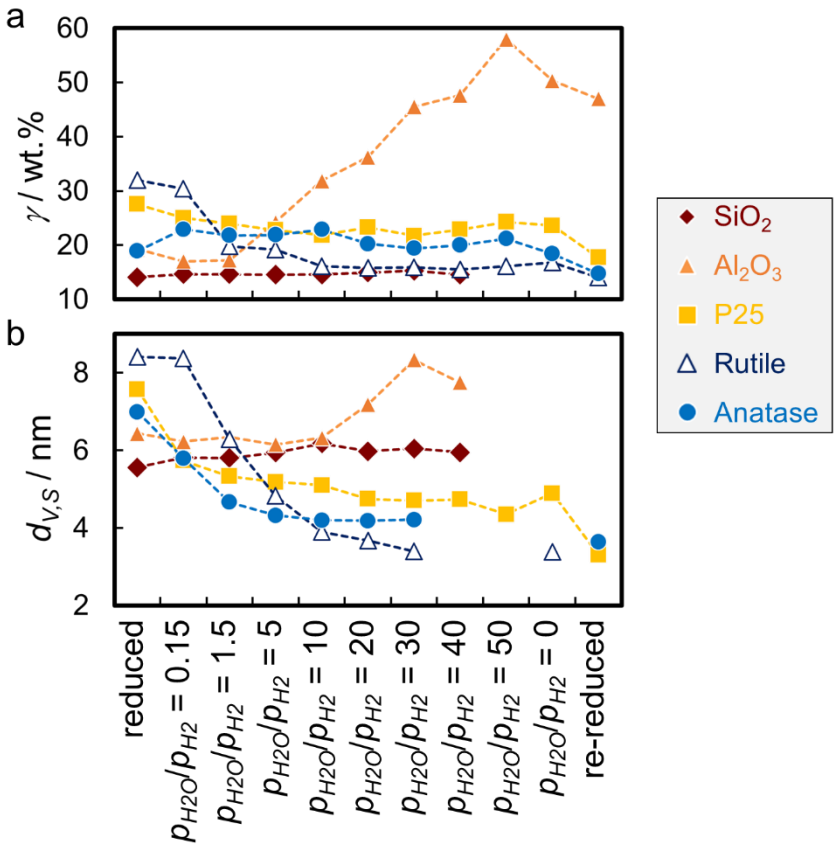

Figure 5. (a) Fraction of cobalt displaying remnant magnetization upon removal of the external field and (b) average cobalt crystallite size of the superparamagnetic fraction, obtained *via* measurement of the magnetization as a function of the external field strength after reduction, exposure to the particular ratios of the partial pressures of water to hydrogen, and re-reduction at 220 °C. Several magnetic hystereses of the model catalysts with a low overall magnetization display a low signal-to-noise ratio, which makes a calculation of the crystallite size unfeasible. The data of the Co/SiO_2 model catalyst is adapted from Wolf *et al.*[12]

The impact of the exposure to H_2O-rich conditions on γ and $d_{V,S}$ for the Co/Al_2O_3 model catalysts differs from the TiO_2-supported catalysts. The γ value increases significantly when oxidation of Co is identified ($p_{H2O}/p_{H2} = 5$) and increases further to almost 60 wt.% during the subsequent H_2O levels (Figure 5a). The average superparamagnetic Co crystallite size also increases with the partial pressure of H_2O (Figure 5b), but the remnant magnetization remains constant during the exposure to simulated high FT conversions (Figure S17). Hence, the increase of the γ value is seemingly related to a preferential oxidation of the smaller superparamagnetic Co crystallites only, while the larger ones display an increased stability against oxidation by H_2O. Relatively large particles are formed in catalyst Co/Al_2O_3 *via* sintering during reduction. In turn, aggregates are most likely situated on the outside of the porous support seeing the small average pore size of 9.6 nm (Figure S13).[73] Hence, the interface area between these large sintered particles and the support is significantly smaller than that for small crystallites situated inside the pores. In turn, the larger particles may only form a limited amount of MSCs, which may explain the different trend in the γ value for the Al_2O_3-supported nanoparticles.

Removing H_2O from the feed stream decreases the γ value in the anatase- and Al_2O_3-supported catalysts (Figure 5a) indicating a preferential re-reduction of smaller cobalt oxide crystallites, which were previously formed during exposure to H_2O-rich environment due to a preferential oxidation of smaller crystallites.[19,21,74] No significant change was observed for supports containing the rutile phase, potentially due to the low reversibility of oxidation.

***In situ* magnetic characterization during re-reduction.** In a final step, the samples were re-reduced in H_2/Ar in order to recover the fraction of oxidized Co, which did not show a thermodynamically controlled reversibility, *i.e.* to fully differentiate between reducible CoO and hard-to-reduce MSCs. Limiting the re-reduction temperature to the final temperature of the initial reduction (360 °C) together with a short holding time can be expected to prevent significant reduction of spectator cobalt oxide species that did not reduce in the initial reduction process (Figure 2).

As some metallic Co was recovered upon removal of H_2O from the feed stream and/or decreasing the pressure (Figure 4), the recovery rate (M_{rec}; ratio of recovered magnetization in the re-reduction over the lost magnetization during exposure to H_2O-rich atmospheres) takes the previously re-reduced Co into account (Equation 4). Less than 7% of oxidized Co could be recovered during re-reduction of the Al_2O_3-, P25-, and rutile-supported model catalysts (Figure 6). The recovery of magnetization is pronounced at lower re-reduction temperatures for the Co/Al_2O_3 model catalyst demonstrating the formation of a cobalt oxide species, which are easier to reduce or less stabilized than in the TiO_2-supported catalysts. The overall recovery rate is less than 20% for all catalysts, *i.e.* more than 80% of the observed loss during exposure to H_2O levels 1-8 can be most likely assigned to the formation of MSCs. This preferential formation of MSCs was expected as the oxidation of Co by H_2O forming CoO is a kinetically hindered process.[14] The anatase-supported catalyst displays the highest recovery rate (Figure 6). However, exposure to H_2O-rich environment only oxidized a small fraction to non-ferromagnetic phases in said catalyst due to the conversion of metallic Co during reduction and the resulting low DOR prior to testing of the stability (Figure 3). A segregation of potentially formed cobalt-titanium species is unlikely due to the low temperatures and would have taken place during the initial reduction as well.[63]

$$M_{rec} = \frac{M_{rev}}{M_{lost}} \cdot 100\% \qquad (4)$$

Where M_{rev} is the fraction of magnetization recovered when H_2O was removed from the feed stream and during re-reduction due to reversible oxidation and M_{lost} is the magnetization lost during co-feeding of H_2O.

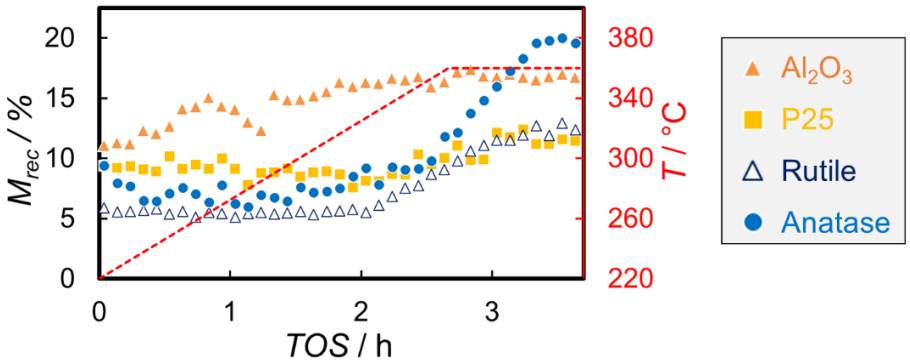

Figure 6. Recovered magnetization at maximum field strength (2 T) during re-reduction relative to the overall loss in magnetization between reduction and the highest water level as a function time on stream and the temperature (dashed). Note that the recovered magnetization upon removal of H_2O from the feed stream and depressurizing of the reactor is given at $TOS = 0$ h.

An observed decrease in the mean crystallite size of superparamagnetic Co crystallites and the γ value upon re-reduction (Figure 5) may be originated in a further re-reduction of smaller cobalt oxide crystallites, but the temperature dependency of the threshold size for superparamagnetism is underlying in these data points as the magnetic hystereses upon re-reduction were measured at 50 °C instead of 220 °C. This temperature dependency can be further demonstrated by comparing the γ values obtained from the magnetic hystereses after reduction at 220 °C (Figure 5a) to the values obtained during reduction at the final holding temperature of 360 °C (Figure S5). While approximately 14-17 wt.% of Co in the model catalysts display remnant magnetization at the end of the reduction at 360 °C, a range of 14-32 wt.% is obtained at 220 °C. As expected, the samples with a larger volume-mean size of superparamagnetic crystallites (Figure 5b) display a pronounced increase in γ. This arises in the correlating temperature dependency of the critical size for superparamagnetism and is more pronounced for wider crystallite size distributions.

***In situ* magnetic characterization during O_2 titration.** Monitoring the magnetization during the final passivation treatment in 1% O_2/Ar[37] can be considered as a titration of the accessible metallic surface in the spent model catalysts (Figure 2). Even the formation of a thin layer of CoO will cause a significant decrease in magnetization.[37] Surprisingly, the magnetization only decreases to a small extent for all model catalysts (<11% of the magnetization prior to passivation) indicating little oxidation by O_2 (Figure S18). Hence, the formation of oxidic species on the surface of the nanoparticles during the preceding exposure to H_2O-rich atmospheres is highly likely. Such species are not expected to reduce during the conducted re-reduction and hence can be expected to represent hard-to-reduce MSCs.

Co/rutile-TiO_2 and Co/Al_2O_3 experience the most pronounced decrease in magnetization during passivation (10-11%). The extent of oxidation approximately matches the amount of Co recovered during re-reduction. However, as all catalysts were re-reduced, a layer that is stable under air atmosphere and hence limits the effect of oxidation during passivation must be protecting the remaining metallic phase in the other catalysts. For example, MSCs may have formed not only at the (initial) interface between the support and the nanoparticle, but also on the Co surface *via* creeping onto the nanoparticle as observed for SiO_2-supported catalysts[18,22] or related diffusion phenomena. Such a formation of cobalt silicates has been reported for Co/Re/SiO_2 catalyst forming needle type structures on the nanoparticles during hydrothermal treatment or high conversion

FTS.[75] More recently, we were able to confirm such a formation on Stöber spheres, which were decorated with different sizes of Co nanoparticles including the Co/SiO_2 model catalyst discussed herein.[22] Needle or platelet type structures were associated to (partially) encapsulated nanoparticles after exposure to simulated high conversion FT environment and identified as cobalt silicates.

The magnetization of the Co/anatase-TiO_2 catalyst decreases by less than 2% during passivation supporting a similar encapsulation of the nanoparticles resulting in a protection of the metallic phase from oxidation, which may be associated with an increase in the mobility of titanium atoms from the support. A pronounced mobility potentially initiated the phase transformation of metallic Co during reduction as well. An increased mobility of metal atoms of the support material has been reported for TiO_2 carriers when compared to the other metal oxide carriers.[48–52] However, the recovered ferromagnetic phase during re-reduction is seemingly not accessible for the O_2 molecules during passivation, which cannot be explained at the current stage.

X-ray absorption near edge structure. XANES analysis of the passivated model catalysts at the Co K-edge provides insight into the different Co phases present. The normalized spectra of the standards for potentially formed MSCs, cobalt oxides, and metallic Co (foil) demonstrate the variety of features associated to the different coordination of Co atoms in the various samples (Figure 7a). Metallic Co has a distinct shoulder on the main edge at 7702 eV, with the main edge at 7709 eV. The oxide references, CoO, Co_3O_4, and cobalt aluminate, have a pre-edge feature at 7701 eV, due to the 1s → 3d transition, this feature is most intense for samples with Co in a tetrahedral environment such as for $CoAl_2O_4$ and weaker for Co in an octahedral environment as in CoO (Table 3).[76] A linear dependency of the edge shift to higher energies with increased valency of the metal[77] has also been reported for Co[39,78,79] and can be confirmed for the cobalt oxide standards.[39] The edge shift of the standards for cobalt silicate and titanate are comparable to the shift in CoO as the valency of Co can be expected to be close to two in both standards.[39] However, cobalt aluminate has a less pronounced edge shift. This is in contrast to an increased valency due to a Co-rich composition of the reference sample resulting in a Co:Al ratio larger than 1:2 ($Co_{1+x}Al_{2-x}O_4$).[39] The pre-edges, the edge shifts, the different intensities and broadenings of the white line for oxidic phases, and unique post-edge features allow for a facile differentiation of the spectra of the standards.

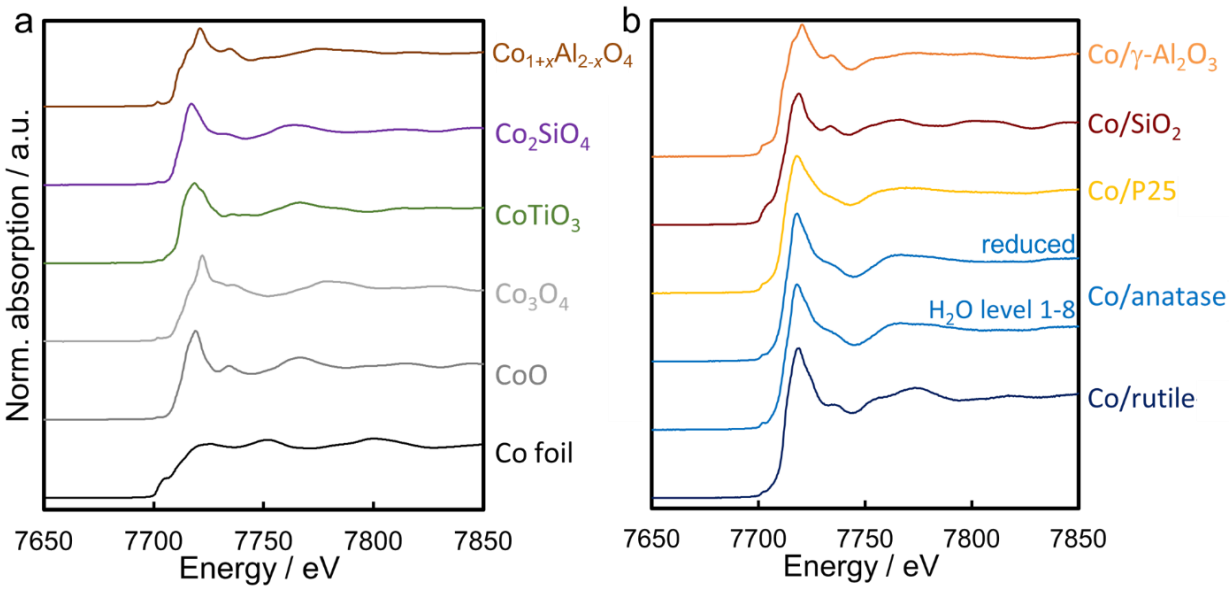

Figure 7. Normalized X-ray absorption near edge structure spectra of (a) standards and (b) spent and passivated model catalysts, as well as passivated model catalyst Co/anatase-TiO_2 after reduction. The spectra of the Co/SiO_2 model catalyst is adapted from Wolf *et al.*[22]

Table 3. Characteristics of the X-ray absorption near edge structure spectra of spent and passivated model catalysts and standards.

Sample	Normalized pre-edge intensity	Edge shift / eV	Normalized white line intensity
CoO	0.04	4.6	1.62
Co_3O_4	0.07	5.7	1.57
$Co_{1+x}Al_{2-x}O_4$	0.09	1.0	1.43
Co/Al_2O_3	0.11	1.3	1.29
Co_2SiO_4	0.06	4.8	1.49
Co/SiO_2	0.22	1.4	1.28
$CoTiO_3$	0.06	3.2	1.47
Co/P25	0.10	2.9	1.34
Co/anatase	0.07	2.2	1.42
Co/anatase, reduced	0.07	3.0	1.44
Co/rutile	0.06	3.0	1.46

Strong differences in the intensity of the pre-edge and the white line can be observed in the XANES spectra obtained for the spent and passivated model catalysts (Figure 7b). The shoulder on the main edge in the spectrum for the Co/SiO_2 catalyst overlaps well with the spectrum of the Co foil.

Further, the reduction in white line intensity when compared to CoO and Co_3O_4 indicates a certain concentration of metallic Co.[22] In contrast, a pre-edge feature can be identified for the TiO_2-supported samples and the white line intensity is more similar to that of the oxide references. These samples also feature a broad white line characteristics similar to the one of the standard for cobalt titanate. Hence, the Co phases in the Co/TiO_2 catalysts can be expected to be mostly oxidic.

Linear combination fitting (LCF) in the first derivative of the normalized absorption is conducted to obtain a quantification of the phase composition for the spent model catalysts (Figure 8). Plotting the spectra and the particular fits in the first derivative improves the visualization of the characteristic features when compared to the normalized absorption. The pronounced shift of the white line of the standard for Co_3O_4 around 7723 eV[80] cannot be identified in any of the samples. Therefore, Co_3O_4 is not present in the passivated samples as reported for the applied passivation technique[37] and in line with the XANES analysis of the spent Co/SiO_2 sample.[22] Nevertheless, Co_3O_4 has been included in additional LCFs, which result in none of the Co atoms being associated to Co_3O_4 demonstrating the absence of this oxide phase in all samples. The presence of CoO can be expected as a fraction of the cobaltous phase was never reduced in the initial reduction and represents a spectator phase during the experiments (Figure 2). Further, additional CoO is exclusively formed during the passivative treatment in 1% O_2/Ar.[37] Hence, CoO, metallic Co, and the particular MSC were selected for LCF of the spent model catalysts (Figure 8).

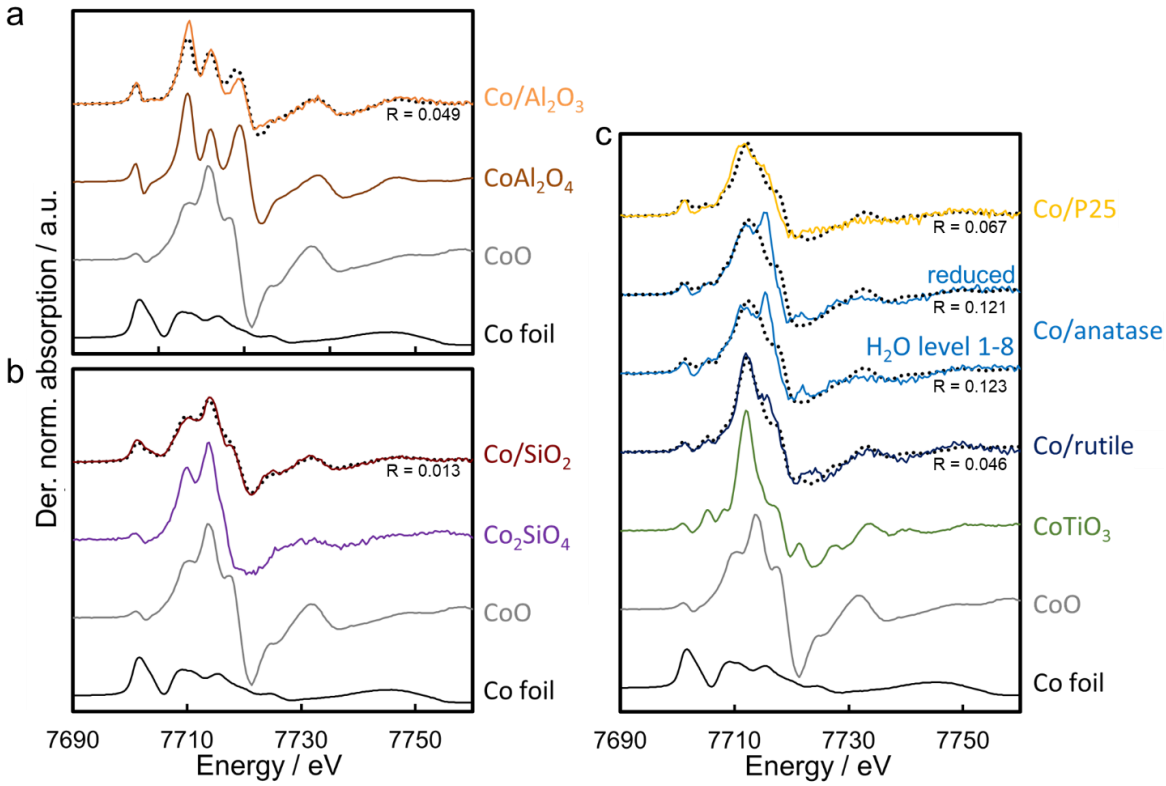

Figure 8. First derivatives of the normalized X-ray absorption near edge structure spectra of the spent and passivated model catalysts with (a) Al_2O_3, (b) Stöber SiO_2 adapted from Wolf *et al.*[22], as well as (c) P25-TiO_2, anatase-TiO_2, rutile-TiO_2 as support material together with the reduced Co/anatase-TiO_2 catalyst and the particular standards. The spectra of the spent catalysts are superimposed with the linear combination fits in the range of -20 to 50 eV relative to the edge (dashed) with the particular standards, while R-factors are given next to the fit.

All characteristics of the first derivative of the experimentally obtained and normalized absorption of Co/Al_2O_3 can be accommodated in a fit with the cobalt aluminate, CoO, and metallic Co standards (Figure 8a) suggesting the absence of additional phases. The fit results in more than half of the Co atoms being associated to cobalt aluminate, while 27% of the Co atoms are present as metallic Co (Table 4). Magnetic measurements during passivation result in a final DOR of 17%, which represents the maximum Co content in the sample as no reduction of oxidic cobalt species is expected during storage of the passivated catalyst under air. In contrast, the metallic fraction in the catalyst may undergo slow, diffusion limited oxidation to CoO.[37] The discrepancy between the DOR upon passivation from the highly sensitive magnetic measurements and the fraction of metallic Co according to the analysis of XANES spectra may demonstrate the semi-quantitative character of the analysis of XANES spectra *via* LCF. Fitting the derivative with CoO, metallic Co, and a bulk-sized cobalt aluminate with a 1:2 ratio of Co:Al results in a worse fit (Figure S19) indicating the formation of Co-rich cobalt aluminate during exposure to H_2O-rich environment, which seemingly has a composition similar to the utilized standard.

Table 4. Degree of reduction of the spent and passivated model catalysts according to magnetic measurement and phase compositions according to the linear combination fitting of X-ray absorption near edge structure spectra with the particular standards in the range of -20 to 50 eV relative to the edge.

Support	Metal oxide	Treatment	DOR_{red} / %	DOR_{pass} / %	Co / %	CoO / %	MSC / %
Puralox	Al_2O_3	H_2O level 1-8, re-red.	44	17	26.8 ± 1.6	19.8 ± 1.5	53.4 ± 2.2
Stöber[a]	SiO_2	H_2O level 1-8	62	53	43.1 ± 0.7	39.1 ± 1.2	17.8 ± 1.4
P25	4:1 a-TiO_2: r-TiO_2	H_2O level 1-8, re-red.	61	32	33.5 ± 1.7	23.5 ± 2.4	43.0 ± 2.9
Anatase	a-TiO_2	-	35	25	22.3 ± 2.5	41.0 ± 3.6	36.7 ± 4.4
Anatase	a-TiO_2	H_2O level 1-8, re-red.	35	32	26.4 ± 2.5	38.1 ± 3.5	35.6 ± 4.3
Rutile	r-TiO_2	H_2O level 1-8, re-red.	68	25	11.8 ± 1.6	25.9 ± 2.3	62.3 ± 2.8

[a] Data for the Co/SiO_2 model catalyst adapted from Wolf *et al*.[22]

Fitting the TiO_2-supported catalysts with the standards for cobalt titanate, CoO, and metallic Co results in high fractions of cobalt titanate (Table 4), but also in rather large errors (Figure 8c). An unfitted peak in the derivative at 7716 eV indicates the presence of an additional phase in the Co/anatase catalysts, which may be present to a lower extent in Co/rutile and Co/P25 as well. No significant difference is identified between the passivated Co/anatase catalysts upon reduction and upon exposure to H_2O-rich environment *via* LCF of XANES spectra. The differences in said samples are potentially limited to the unidentified cobaltous species. The fit of the first derivative of the spent Co/SiO_2 only deviates marginally from the experimental spectra (Figure 8b) and results in 18% of Co atoms being coordinated as cobalt silicate (Table 4).[22]

Comparing the amount of CoO from LCF with the amount of CoO present after the initial reduction provides insight into the role of non-reduced CoO during exposure to H_2O-rich environment. Passivation of the catalysts resulted in little oxidation of the samples (Figure S18), while the solid-state reaction of CoO with the metal oxide carriers is highly likely (Figure 1c) and decreases the CoO content in the catalysts. For the Co/SiO_2 catalyst, the amount of CoO from LCF (39.1% of Co atoms are associated to CoO) matches the fraction of cobalt oxide species present after the initial reduction (100% - DOR_{red} = 38%; Table 4). LCF for the other catalysts results in significantly lower fractions of CoO than after reduction. Hence, the unreduced CoO fraction cannot be considered a spectator species during exposure to H_2O-rich atmospheres. This observation strongly supports the formation of MSCs from CoO aside from to the identified formation of MSCs from the metallic phase (Figure 2). The latter direct formation of MSCs has previously been hypothesized to be kinetically hindered for the formation of cobalt aluminates, which was suggested to proceed *via* CoO as an intermediate only.[10] Several studies adopted said hypothesis, which may have resulted in erroneous conclusions.[13,26,64,81,82] Besides the relative high p_{H2O}/p_{H2} ratios, the absence of a calcination step may have been the key allowing for the observation of formation of MSC from the metallic Co phase. The formation may be hindered in a calcined catalyst due the formation of MSCs during the catalyst preparation. A relatively thick oxidic layer between the metallic Co and the support providing pronounced metal-support interaction may also prevent significant diffusion of Co into the support. Such a (mixed) metal oxide layer, if present at all upon reduction of the anchored nanoparticles, can be expected to be thinner in the present study as no strong metal-support interactions have been induced during the preparation of the catalyst.

In order to further investigate the potential formation of a cobalt-titanium alloy, additional EXAFS spectra were modelled in Artemis.[42] Various compositions were taken into account resulting in similar spectra (Figure 9). However, comparison of the modelled and experimentally obtained spectra for Co demonstrates the prominent characteristics in the modelled spectra featuring narrow peaks. Nevertheless, LCF of the XANES spectra of the spent and passivated catalysts was conducted from -20 to 20 eV relative to the edge including one of the cobalt-titanium alloy compositions in addition to the previously utilized standards. Only LCF including Co_3Ti resulted in viable fits (Figure S20). Between 3 and 13% of the Co atoms were associated to the alloy (Table S2) improving the residual of the fits significantly. As expected, the highest fractions of the alloy were observed for the anatase support, followed by rutile and P25, *i.e.* the trend in the three different catalyst systems strengthens the hypothesized presence of Co_3Ti.

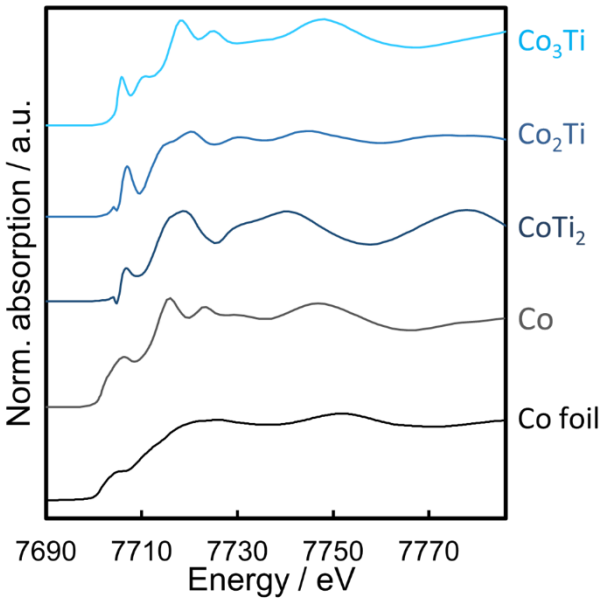

Figure 9. Modelled and normalized X-ray absorption near edge structure spectra for cobalt-titanium alloys and fcc-cobalt with the experimentally obtained spectra of cobalt foil.

High-resolution scanning transmission electron microscopy. The spent and passivated model catalysts were analyzed by HRSTEM with elemental mapping *via* EELS imaging. The low Co loading and the crystalline support materials complicate the identification of formed MSCs or even Co crystallites in the Al_2O_3- and TiO_2-supported samples. Needle- or platelet-type cobalt silicate structures have been previously identified on the Co/SiO_2 catalyst[22] being in line with literature.[75] MSCs with a much higher concentration have been identified in the other samples *via* XAS as well. However, the high conversion of metallic Co into oxidic phases in the present study and the special morphology of formed MSCs with highly dispersed Co atoms may result in low concentrations of metallic Co atoms and thus a low contrast between the support and MSCs. Such a morphology has been successfully identified in the Al_2O_3-supported sample (Figure 10). An elemental map for Co, as obtained *via* EELS imaging, follows the contrast observed in the high angle annular dark field micrograph suggesting the formation of a dispersed Co phase on or within the Al_2O_3 support. The small scale of the Co-rich areas (< 2 nm) strengthens this hypothesis. Tsakoumis *et al.* recently suggested a similar formation of a highly dispersed cobalt aluminate phase for small Co crystallites, which firstly oxidize to CoO prior to formation of MSCs.[13] Such a process *via* wetting of the nanoparticles followed by diffusion into the support structure may have been at play in the herein characterized model catalysts as well. In contrast to the suggested mechanism by Tsakoumis *et al.*, a (mostly) direct formation of MSCs from the metallic Co phase has been observed in the present study. Elemental mapping strongly suggests the formation of flat nano-sized cobaltous domains on the support (Figure 10). Hence, the direct solid-state reaction of metallic Co with the support material in the presence of H_2O is suggested to result in such structures (Figure 11).

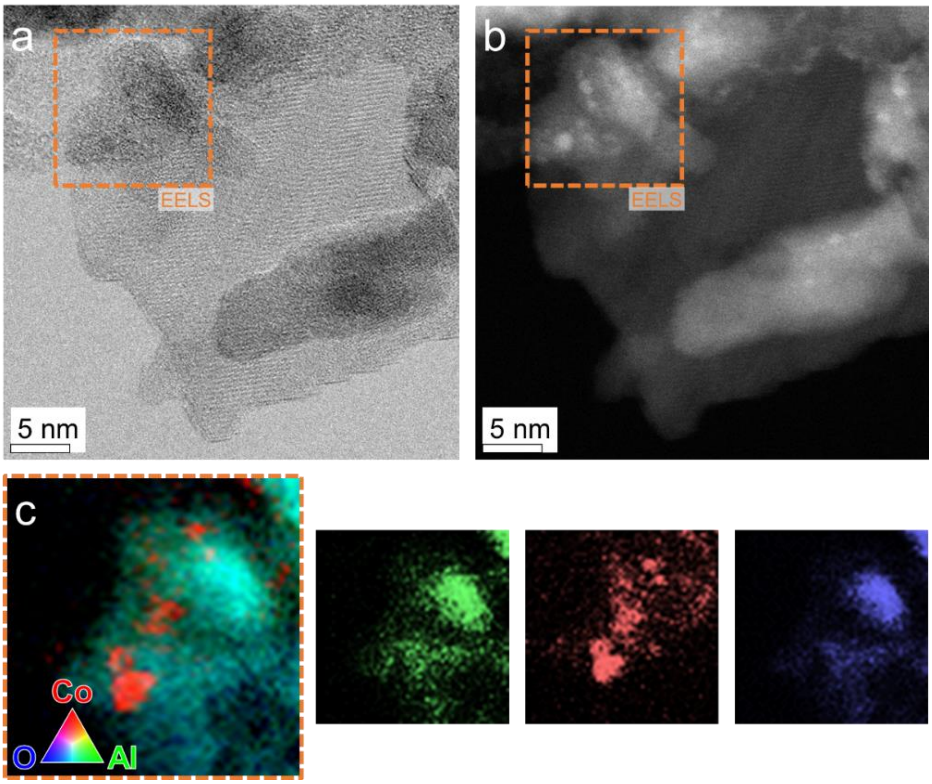

Figure 10. High-resolution (a) bright field and (b) high angle annular dark field scanning transmission electron micrographs of the spent and passivated alumina-supported model catalyst with (c) elemental mapping as obtained *via* electron energy loss spectroscopy with separate maps for the particular elements.

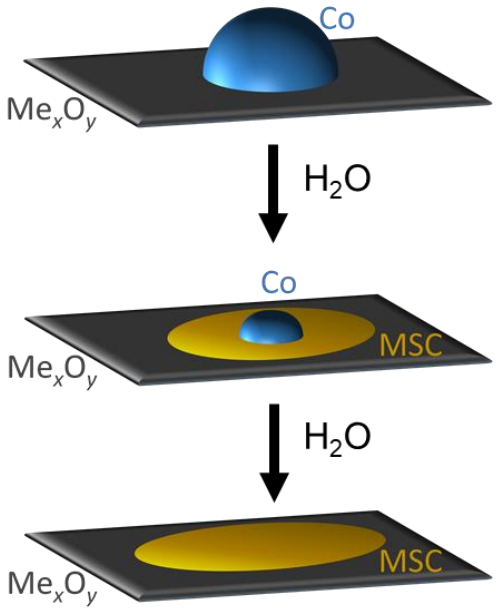

Figure 11. Schematic of the proposed mechanism of the direct transformation of metallic cobalt to cobalt-support compounds by water for titania- and alumina-supported nanoparticles *via* wetting and diffusion into the support structure.

Analysis of the TiO_2-supported catalysts after exposure to H_2O-rich environment by means of HRSTEM coupled with EELS imaging exhibits similar structures of a highly dispersed Co phase within a relatively large area surrounding a Co-rich domain (Figure 12; Figures S21 and S22). Exposure of the model catalysts to p_{H2O}/p_{H2} ratios up to 50 may also induce complete oxidation of the larger Co nanoparticles via continuous diffusion of the oxidized cobalt into the support to form MSCs within the said structure (Figure 11). Concentration gradients can be expected for such structures with a Co-rich MSC in close vicinity to the (former) center of the nanoparticle and lower concentrations of Co within the structure of the MSC surrounding this highly saturated area. Such gradients may provide an explanation for the challenging LCF of XANES spectra with standards as more than one standard would be required, *i.e.* at least a Co-rich and a Co-poor standard for the particular MSCs. In contrast to the amorphous SiO_2 Stöber spheres, the diffusion of Co atoms into the support lattice structure would then be the dominating process during the H_2O-induced formation of MSCs in the utilized TiO_2 and Al_2O_3 supports.

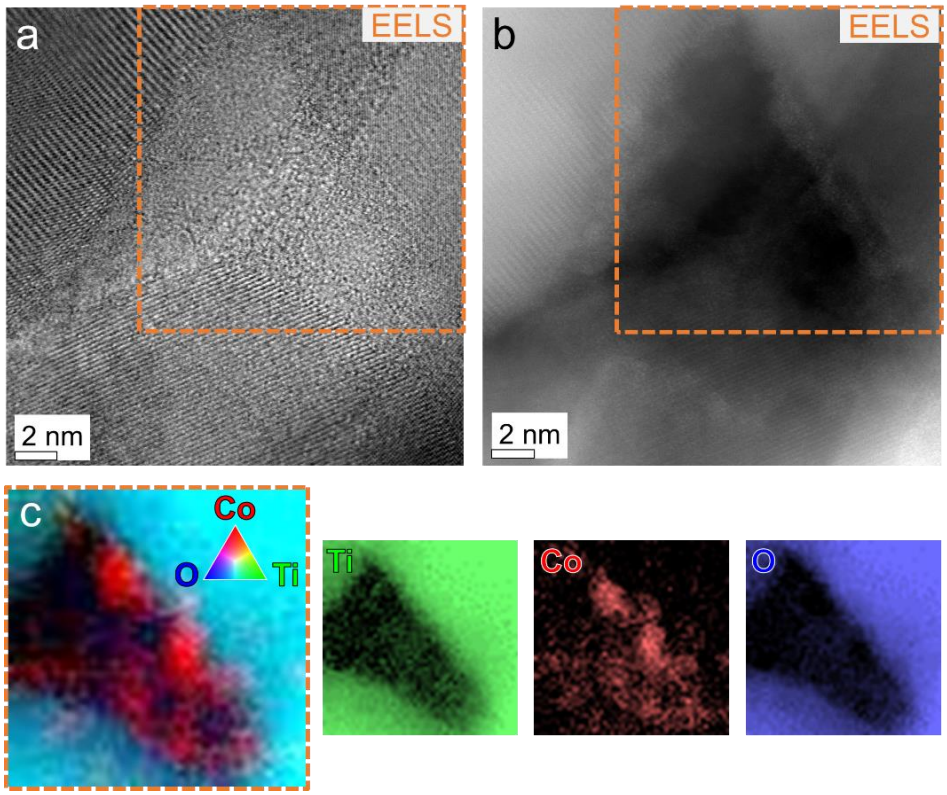

Figure 12. High-resolution (a) bright field and (b) high angle annular dark field scanning transmission electron micrographs of the spent and passivated P25-supported model catalyst with (c) elemental mapping as obtained *via* electron energy loss spectroscopy with separate maps for the particular elements.

SUMMARY AND CONCLUSION

In a comparative study, well-defined Co_3O_4 nanoparticles were deposited on Puralox Al_2O_3 and three TiO_2 carriers, namely the commercial mixed-phase TiO_2 support P25, as well as single-phase anatase and rutile. The stability of the nanoparticles during reduction to Co and subsequent

exposure to simulated high FT conversion levels was monitored using an *in situ* magnetometer and compared to the same nanoparticles supported on SiO_2 Stöber spheres from a previous study on the size dependent oxidation behavior of nano-sized Co.

In accordance with conducted thermodynamic predictions for the bulk-phase solid-state reactions between Co and the support materials, Co/SiO_2 was found to be the most stable system. However, creeping of SiO_2 species has been identified resulting in coverage of metallic Co nanoparticles. TiO_2-supported Co nanoparticles readily formed high amounts of cobalt-support compounds at low partial pressure ratios of H_2O to H_2 corresponding to industrially relevant conversion levels of the FTS. Furthermore, in the case of anatase, such MSCs even formed during reduction in H_2/Ar. Even though thermodynamic predictions suggest such a high instability of metallic Co on TiO_2 at low concentrations of H_2O, the vast formation of MSCs was unexpected due to a successful application of TiO_2 as carrier material in the commercial FTS. However, the herein prepared and tested model catalyst cannot be compared to a fully engineered commercial FT catalyst with promoters and additives for both, the active Co phase and the support material. Commercial Co/TiO_2 catalysts potentially tolerate the formation of a small amount of MSCs during preparation and/or operation as significantly larger Co loadings are applied. In contrast to the Co/TiO_2 sample, the Co/Al_2O_3 model catalyst was stable at industrially relevant conditions. Cobalt aluminates formed in a kinetically hindered process at increased simulated conversion levels. This observation is contradictory to thermodynamic calculations, which suggest a spontaneous oxidation at low concentration levels of H_2O.

The hard-to-reduce MSCs were characterized by means of XANES and HRSTEM. In accordance to the *in situ* magnetic measurements, large fractions of cobalt aluminate and titanate were identified. Interestingly, the spent titania-supported catalysts seemingly feature another species, potentially a cobalt-titanium alloy, which may have formed during reduction of oxidic cobalt on anatase as well. Elemental mapping *via* EELS suggests a wetting of the nanoparticles over the support followed by formation of the MSCs.

The herein presented results show a high significance for fundamental research on the FTS, FT catalyst design, and industrial application of Co-based catalysts in the FTS alike. The observed formation of MSCs from the metallic phase can be considered as the maximum potential for such phase transitions as the catalysts, aside from the Co/anatase sample, do not comprise such MSCs upon reduction and oxidation to CoO during exposure to H_2O-rich atmospheres was limited by the absence of CO. Hence, impregnated and calcined catalysts are expected to form less MSCs, while realistic FT conditions including the reactant CO may result in deactivation of Co *via* oxidation to CoO prior to the formation of MSCs. Nevertheless, the presented results suggest utilization of Al_2O_3 as the carrier of choice in the FTS for conversion levels below 75% in order to minimize potential deactivation of Co *via* water-induced direct formation of MSCs.

ASSOCIATED CONTENT

Supporting Information. Details on Jiles-Atherton method and an exemplary application on a measured hysteresis, XRD analysis, nitrogen adsorption-desorption isotherms, pore size distributions, TEM images of the support materials, extended data of the *in situ* magnetic characterization, alternative LCF fitting of XANES spectra, HRSTEM and EELS analysis of the spent single-phase titania-supported catalysts (PDF)

AUTHOR INFORMATION

Corresponding Author
*Correspondence should be addressed to M. Claeys (E-mail: michael.claeys@uct.ac.za).

NOTES

The authors declare no competing financial interest.

ACKNOWLEDGMENT

Financial support from the DST-NRF Centre of Excellence in Catalysis (c*change), the UK Catalysis Hub, the University of Cape Town (UCT), the University College London (UCL), and the German Academic Exchange Service (DAAD) is gratefully acknowledged. Special thanks go to S. La Grange, Z. Le Riche, and R. Geland of the Analytical Laboratory in the Department of Chemical Engineering at UCT for conducting the physisorption experiments and the elemental analyses. Anna Petersen of the Catalysis Institute and c*change at UCT is kindly acknowledged for the preparation of co-precipitated bulk-phased $CoAl_2O_4$. Lastly, Dr. Diego Gianolio from the Diamond Light Source is acknowledged for modelling extended X-ray absorption fine structure spectra.

ABBREVIATIONS

DOR, degree of reduction; EELS, electron energy loss spectroscopy; EXAFS, extended X-ray absorption fine structure; FT, Fischer-Tropsch; FTS, Fischer-Tropsch synthesis; GHSV, gas hourly space velocity; HRSTEM, high-resolution scanning transmission electron microscopy; ICP-OES, inductively coupled plasma optical emission spectrometry; LCF, linear combination fitting; MSC, metal-support compound; TEM, transmission electron microscopy; TPR, temperature programed reduction; XAS, X-ray absorption spectroscopy; XANES, X-ray absorption near edge structure; XRD, X-ray diffraction.

REFERENCES

(1) Bartholomew, C. H. Mechanisms of Catalyst Deactivation. *Appl. Catal. A Gen.* **2001**, *212*, 17–60.
(2) Bezemer, G. L.; Remans, T. J.; van Bavel, A. P.; Dugulan, A. I. Direct Evidence of Water-Assisted Sintering of Cobalt on Carbon Nanofiber Catalysts during Simulated Fischer-Tropsch Conditions Revealed with in Situ Mössbauer Spectroscopy. *J. Am. Chem. Soc.* **2010**, *132*, 8540–8541.
(3) Sadeqzadeh, M.; Hong, J.; Fongarland, P.; Curulla-Ferré, D.; Luck, F.; Bousquet, J.;

Schweich, D.; Khodakov, A. Y. Mechanistic Modeling of Cobalt Based Catalyst Sintering in a Fixed Bed Reactor under Different Conditions of Fischer-Tropsch Synthesis. *Ind. Eng. Chem. Res.* **2012**, *51*, 11955–11964.

(4) Claeys, M.; Dry, M. E.; van Steen, E.; van Berge, P. J.; Booyens, S.; Crous, R.; van Helden, P.; Labuschagne, J.; Moodley, D. J.; Saib, A. M. Impact of Process Conditions on the Sintering Behavior of an Alumina-Supported Cobalt Fischer-Tropsch Catalyst Studied with an in Situ Magnetometer. *ACS Catal.* **2015**, *5*, 841–852.

(5) Dry, M. E. FT Catalysts. In *Fischer-Tropsch Technology*; Steynberg, A. P., Dry, M. E., Eds.; Studies in Surface Science and Catalysis; Elsevier: Amsterdam, 2004; Vol. 152, pp 533–600.

(6) Dalai, A. K.; Davis, B. H. Fischer-Tropsch Synthesis: A Review of Water Effects on the Performances of Unsupported and Supported Co Catalysts. *Appl. Catal. A Gen.* **2008**, *348*, 1–15.

(7) Tsakoumis, N. E.; Rønning, M.; Borg, Ø.; Rytter, E.; Holmen, A. Deactivation of Cobalt Based Fischer-Tropsch Catalysts: A Review. *Catal. Today* **2010**, *154*, 162–182.

(8) Rytter, E.; Holmen, A. Deactivation and Regeneration of Commercial Type Fischer-Tropsch Co-Catalysts - A Mini-Review. *Catalysts* **2015**, *5*, 478–499.

(9) van Rensburg, W. J.; van Helden, P.; Moodley, D. J.; Claeys, M.; Petersen, M. A.; Van Steen, E. The Role of Transient Co-Subcarbonyls in Ostwald Ripening Sintering of Cobalt Supported on γ-Alumina Surfaces. *J. Phys. Chem. C* **2017**, *121*, 16739–16753.

(10) van Berge, P. J.; van de Loosdrecht, J.; Barradas, S.; van der Kraan, A. M. Oxidation of Cobalt Based Fischer-Tropsch Catalysts as a Deactivation Mechanism. *Catal. Today* **2000**, *58*, 321–334.

(11) van de Loosdrecht, J.; Balzhinimaev, B.; Dalmon, J.-A.; Niemantsverdriet, J. W.; Tsybulya, S. V.; Saib, A. M.; van Berge, P. J.; Visagie, J. L. Cobalt Fischer-Tropsch Synthesis: Deactivation by Oxidation? *Catal. Today* **2007**, *123*, 293–302.

(12) Wolf, M.; Kotzé, H.; Fischer, N.; Claeys, M. Size Dependent Stability of Cobalt Nanoparticles on Silica under High Conversion Fischer-Tropsch Environment. *Faraday Discuss.* **2017**, *197*, 243–268.

(13) Tsakoumis, N. E.; Walmsley, J. C.; Rønning, M.; van Beek, W.; Rytter, E.; Holmen, A. Evaluation of Re-Oxidation Thresholds for γ-Al_2O_3 Supported Cobalt Catalysts under Fischer-Tropsch Synthesis Conditions. *J. Am. Chem. Soc.* **2017**, *139*, 3706–3715.

(14) Wolf, M.; Mutuma, B. K.; Coville, N. J.; Fischer, N.; Claeys, M. Role of CO in the Water-Induced Formation of Cobalt Oxide in a High Conversion Fischer-Tropsch Environment. *ACS Catal.* **2018**, *8*, 3985–3989.

(15) Filot, I. A. W.; van Santen, R. A.; Hensen, E. J. M. The Optimally Performing Fischer-Tropsch Catalyst. *Angew. Chemie Int. Ed.* **2014**, *53*, 12746–12750.

(16) Kizilkaya, A. C.; Niemantsverdriet, J. W.; Weststrate, C. J. Oxygen Adsorption and Water Formation on Co(0001). *J. Phys. Chem. C* **2016**, *120*, 4833–4842.

(17) van Helden, P.; van den Berg, J.-A.; Petersen, M. A.; van Rensburg, W. J.; Ciobîcă, I. M.; van de Loosdrecht, J. Computational Investigation of the Kinetics and Mechanism of the Initial Steps of the Fischer–Tropsch Synthesis on Cobalt. *Faraday Discuss.* **2017**, *197*, 117–151.

(18) Saib, A. M.; Borgna, A.; van de Loosdrecht, J.; van Berge, P. J.; Geus, J. W.; Niemantsverdriet, J. W. Preparation and Characterisation of Spherical Co/SiO_2 Model Catalysts with Well-Defined Nano-Sized Cobalt Crystallites and a Comparison of Their

Stability against Oxidation with Water. *J. Catal.* **2006**, *239*, 326–339.
(19) van Steen, E.; Claeys, M.; Dry, M. E.; van de Loosdrecht, J.; Viljoen, E. L.; Visagie, J. L. Stability of Nanocrystals: Thermodynamic Analysis of Oxidation and Re-Reduction of Cobalt in Water/Hydrogen Mixtures. *J. Phys. Chem. B* **2005**, *109*, 3575–3577.
(20) van de Loosdrecht, J.; Botes, F. G.; Ciobîcă, I. M.; Ferreira, A.; Gibson, P.; Moodley, D. J.; Saib, A. M.; Visagie, J. L.; Weststrate, C. J.; Niemantsverdriet, J. W. Fischer-Tropsch Synthesis: Catalysts and Chemistry. In *Comprehensive Inorganic Chemistry II (Second Edition): From Elements to Applications*; Elsevier Ltd., 2013; Vol. 7, pp 525–557.
(21) Fischer, N.; Clapham, B.; Feltes, T.; van Steen, E.; Claeys, M. Size-Dependent Phase Transformation of Catalytically Active Nanoparticles Captured in Situ. *Angew. Chemie Int. Ed.* **2014**, *53*, 1342–1345.
(22) Wolf, M.; Gibson, E. K.; Olivier, E. J.; Neethling, J. H.; Catlow, C. R. A.; Fischer, N.; Claeys, M. In-Depth Characterisation of Metal-Support Compounds in Spent Co/SiO2 Fischer-Tropsch Model Catalysts. *Catal. Today* **2019**, in press, DOI: 10.1016/j.cattod.2019.01.065.
(23) *Thermochemical Properties of Inorganic Substances*, 2nd ed.; Knacke, O., Kubaschewski, O., Hesselmann, K., Eds.; Springer: Berlin, 1991.
(24) Bolt, P. H.; Habraken, F. H. P. M.; Geus, J. W. Formation of Nickel, Cobalt, Copper, and Iron Aluminates from α- and γ-Alumina-Supported Oxides: A Comparative Study. *J. Solid State Chem.* **1998**, *135*, 59–69.
(25) Hou, C.; Xia, G.; Sun, X.; Wu, Y.; Jin, C.; Yan, Z.; Li, M.; Hu, Z.; Nie, H.; Li, D. Thermodynamics of Oxidation of an Alumina-Supported Cobalt Catalyst by Water in F-T Synthesis. *Catal. Today* **2016**, *264*, 91–97.
(26) Moodley, D. J.; Saib, A. M.; van de Loosdrecht, J.; Welker-Nieuwoudt, C. A.; Sigwebela, B. H.; Niemantsverdriet, J. W. The Impact of Cobalt Aluminate Formation on the Deactivation of Cobalt-Based Fischer-Tropsch Synthesis Catalysts. *Catal. Today* **2011**, *171*, 192–200.
(27) Wolf, M.; Fischer, N.; Claeys, M. Surfactant-Free Synthesis of Monodisperse Cobalt Oxide Nanoparticles of Tunable Size and Oxidation State Developed by Factorial Design. *Mater. Chem. Phys.* **2018**, *213*, 305–312.
(28) Shi, N.; Cheng, W.; Zhou, H.; Fan, T.; Niederberger, M. Facile Synthesis of Monodisperse Co_3O_4 Quantum Dots with Efficient Oxygen Evolution Activity. *Chem. Commun.* **2015**, *51*, 1338–1340.
(29) Claeys, M.; van Steen, E.; Visagie, J. L.; van de Loosdrecht, J. Magnetometer. US Patent 8,773,118 B2, 2014.
(30) Dalmon, J.-A. Magnetic Measurements and Catalysis. In *Catalyst Characterization: Physical Techniques for Solid Materials*; Imelik, B., Vedrine, J. C., Eds.; Fundamental and Applied Catalysis; Plenum Press: New York, 1994; pp 585–609.
(31) Sechovsky, V. Magnetism in Solids : General Introduction. In *Encyclopedia of Materials: Science and Technology*; Buschow, K. H. J., Cahn, R. W., Flemings, M. C., Ilschner, B., Kramer, E. J., Mahajan, S., Eds.; Elsevier: Amsterdam, 2001; Vol. 5, pp 5018–5032.
(32) Holt, K.; Jewell, L.; Niemantsverdriet, H.; Macheli, L.; Shozi, M.; Hutchings, G.; Wezendonk, T.; Bowker, M.; Catlow, R.; Adam, S.; Kooyman, P. J.; Hensen, E.; Hayward, J.; Coville, N.; Weststrate, K.-J.; Fischer, N.; Roldan, A.; Redekop, E.; van Steen, E.; Friedrich, H.; Kuo, D.-H.; Bandaru, H.; Deeplal, L.; Zivkovic, A.; Naiker, K.; Tucker, C.; Mkhwanazi, T. P. O.; Bahnemann, D.; Neurock, M.; Petersen, A.; Forbes, R. P.;

Phaahlamohlaka, T.; Schulz, H.; Lennon, D.; Olsbye, U.; Wolf, M.; Kondrat, S.; Collier, P.; Sun, X.; Zheng, Y.; Corma, A.; Iglesia, E.; Nyathi, T.; Ma, D.; Bremmer, M.; Claeys, M.; Kapteijn, F. Designing New Catalysts for Synthetic Fuels: General Discussion. *Faraday Discuss.* **2017**, *197*, 353–388.

(33) Barbier, A.; Hanif, A.; Dalmon, J.-A.; Martin, G. A. Preparation and Characterization of Well-Dispersed and Stable Co/SiO_2 Catalysts Using the Ammonia Method. *Appl. Catal. A Gen.* **1998**, *168*, 333–343.

(34) Barbier, A.; Martin, G.-A.; Ramirez de la Piscina, P.; Homs, N. Co/SiO_2 Catalysts Prepared from $Co_2(CO)_8$ for CO Hydrogenation into Alcohols and Hydrocarbons: Characterization by Magnetic Methods and Temperature-Programmed Hydrogenation. *Appl. Catal. A Gen.* **2001**, *210*, 75–81.

(35) Jiles, D. C.; Atherton, D. L. Theory of Ferromagnetic Hysteresis (Invited). *J. Appl. Phys.* **1984**, *55*, 2115–2120.

(36) Jiles, D. C.; Atherton, D. L. Theory of Ferromagnetic Hysteresis. *J. Magn. Magn. Mater.* **1986**, *61*, 48–60.

(37) Wolf, M.; Fischer, N.; Claeys, M. Effectiveness of Catalyst Passivation Techniques Studied in Situ with a Magnetometer. *Catal. Today* **2016**, *275*, 135–140.

(38) Karmaoui, M.; Silva, N. J. O.; Amaral, V. S.; Ibarra, A.; Millán, Á.; Palacio, F. Synthesis of Cobalt Aluminate Nanopigments by a Non-Aqueous Sol-Gel Route. *Nanoscale* **2013**, *5*, 4277–4283.

(39) Wolf, M.; Roberts, S. J.; Olivier, E. J.; Luchters, T. J.; Gibson, E. K.; Catlow, C. R. A.; Neethling, J. H.; Fischer, N.; Claeys, M. Synthesis, characterisation and water-gas shift activity of nano-particulate mixed-metal (Al, Ti) cobalt oxides. *ChemRxiv* **2019**, pre-print, DOI: 10.26434/chemrxiv.8009591.

(40) Bruce, L. A.; Sanders, J. V.; Turney, T. W. Hydrothermal Synthesis and Characterization of Cobalt Clays. *Clays Clay Miner.* **1986**, *34*, 25–36.

(41) Dent, A. J.; Cibin, G.; Ramos, S.; Smith, A. D.; Scott, S. M.; Varandas, L.; Pearson, M. R.; Krumpa, N. A.; Jones, C. P.; Robbins, P. E. B18: A Core XAS Spectroscopy Beamline for Diamond. *J. Phys. Conf. Ser.* **2009**, *190*, 012039.

(42) Ravel, B.; Newville, M. ATHENA, ARTEMIS, HEPHAESTUS: Data Analysis for X-Ray Absorption Spectroscopy Using IFEFFIT. *J. Synchrotron Radiat.* **2005**, *12*, 537–541.

(43) Newville, M. IFEFFIT: Interactive XAFS Analysis and FEFF Fitting. *J. Synchrotron Radiat.* **2001**, *8*, 322–324.

(44) ICDD. *PDF-2 Release 2008 (Database)*; Kabekkodu, S., Ed.; International Centre for Diffraction Data: Newtown Square, USA, 2008.

(45) Coelho, A. A. Indexing of Powder Diffraction Patterns by Iterative Use of Singular Value Decomposition. *J. Appl. Crystallogr.* **2003**, *36*, 86–95.

(46) Scherrer, P. Bestimmung Der Größe Und Der Inneren Struktur von Kolloidteilchen Mittels Röntgenstrahlen. *Nachrichten von der Gesellschaft der Wissenschaften zu Göttingen, Math. Klasse* **1918**, 98–100.

(47) Bergeret, G.; Gallezot, P. Particle Size and Dispersion Measurements. In *Handbook of Heterogeneous Catalysis*; Ertl, G., Knözinger, H., Schüth, F., Weitkamp, J., Eds.; Wiley-VCH: Weinheim, Germany, 2008; pp 738–765.

(48) Conesa, J. C.; Soria, J. Reversible Ti^{3+} Formation by H_2 Adsorption on M/TiO_2 Catalysts. *J. Phys. Chem.* **1982**, *86*, 1392–1395.

(49) Huizinga, T.; van Grondelle, J.; Prins, R. A Temperature Programmed Reduction Study of

Pt on Al_2O_3 and TiO_2. *Appl. Catal.* **1984**, *10*, 199–213.
(50) Haller, G. L.; Resasco, D. E. Metal-Support Interaction: Group VIII Metals and Reducible Oxides. *Adv. Catal.* **1989**, *36*, 173–235.
(51) Li, Y.; Fan, Y.; Yang, H.; Xu, B.; Feng, L.; Yang, M.; Chen, Y. Strong Metal-Support Interaction and Catalytic Properties of Anatase and Rutile Supported Palladium Catalyst Pd/TiO_2. *Chem. Phys. Lett.* **2003**, *372*, 160–165.
(52) Panagiotopoulou, P.; Christodoulakis, A.; Kondarides, D. I.; Boghosian, S. Particle Size Effects on the Reducibility of Titanium Dioxide and Its Relation to the Water-Gas Shift Activity of Pt/TiO_2 Catalysts. *J. Catal.* **2006**, *240*, 114–125.
(53) Karim, W.; Spreafico, C.; Kleibert, A.; Gobrecht, J.; VandeVondele, J.; Ekinci, Y.; van Bokhoven, J. A. Catalyst Support Effects on Hydrogen Spillover. *Nature* **2017**, *541*, 68–71.
(54) Prins, R. Hydrogen Spillover. Facts and Fiction. *Chem. Rev.* **2012**, *112*, 2714–2738.
(55) Roland, U.; Braunschweig, T.; Roessner, F. On the Nature of Spilt-over Hydrogen. *J. Mol. Catal. A Chem.* **1997**, *127*, 61–84.
(56) Nabaho, D.; Niemantsverdriet, J. W.; Claeys, M.; van Steen, E. Hydrogen Spillover in the Fischer-Tropsch Synthesis: An Analysis of Platinum as a Promoter for Cobalt-Alumina Catalysts. *Catal. Today* **2015**, *261*, 17–27.
(57) Jongsomjit, B.; Sakdamnuson, C.; Praserthdam, P. Dependence of Crystalline Phases in Titania on Catalytic Properties during CO Hydrogenation of Co/TiO_2 Catalysts. *Mater. Chem. Phys.* **2005**, *89*, 395–401.
(58) Jongsomjit, B.; Wongsalee, T.; Praserthdam, P. Study of Cobalt Dispersion on Titania Consisting Various Rutile:Anatase Ratios. *Mater. Chem. Phys.* **2005**, *92*, 572–577.
(59) Jongsomjit, B.; Wongsalee, T.; Praserthdam, P. Characteristics and Catalytic Properties of Co/TiO_2 for Various Rutile:Anatase Ratios. *Catal. Commun.* **2005**, *6*, 705–710.
(60) Newnham, R. E.; Fang, J. H.; Santoro, R. P. Crystal Structure and Magnetic Properties of $CoTiO_3$. *Acta Crystallogr.* **1964**, *17*, 240–242.
(61) Aoki, Y.; Nakamichi, T.; Yamamoto, M. Magnetic Properties of Cobalt-Titanium Alloys with the CsCl-Type Structure. *J. Phys. Soc. Japan* **1969**, *27*, 1455–1458.
(62) Aboaf, J. A.; Klokholm, E. Amorphous Magnetic Alloys of Cobalt-Titanium. *J. Appl. Phys.* **1981**, *52*, 1844–1846.
(63) Murray, J. L. The Co-Ti (Cobalt-Titanium) System. *Bull. Alloy Phase Diagrams* **1982**, *3*, 74–85.
(64) Li, J.; Zhan, X.; Zhang, Y.; Jacobs, G.; Das, T.; Davis, B. H. Fischer-Tropsch Synthesis: Effect of Water on the Deactivation of Pt Promoted Co/Al_2O_3 Catalysts. *Appl. Catal. A Gen.* **2002**, *228*, 203–212.
(65) Li, J.; Jacobs, G.; Das, T.; Davis, B. H. Fischer-Tropsch Synthesis: Effect of Water on the Catalytic Properties of a Ruthenium Promoted Co/TiO_2 Catalyst. *Appl. Catal. A Gen.* **2002**, *233*, 255–262.
(66) Li, J.; Jacobs, G.; Das, T.; Zhang, Y.; Davis, B. Fischer-Tropsch Synthesis: Effect of Water on the Catalytic Properties of a Co/SiO_2 Catalyst. *Appl. Catal. A Gen.* **2002**, *236*, 67–76.
(67) Storsæter, S.; Tøtdal, B.; Walmsley, J. C.; Tanem, B. S.; Holmen, A. Characterization of Alumina-, Silica-, and Titania-Supported Cobalt Fischer-Tropsch Catalysts. *J. Catal.* **2005**, *236*, 139–152.
(68) Jacobs, G.; Das, T. K.; Zhang, Y.; Li, J.; Racoillet, G.; Davis, B. H. Fischer-Tropsch Synthesis: Support, Loading, and Promoter Effects on the Reducibility of Cobalt Catalysts. *Appl. Catal. A Gen.* **2002**, *233*, 263–281.

(69) Jacobs, G.; Ji, Y.; Davis, B. H.; Cronauer, D.; Kropf, A. J.; Marshall, C. L. Fischer-Tropsch Synthesis: Temperature Programmed EXAFS/XANES Investigation of the Influence of Support Type, Cobalt Loading, and Noble Metal Promoter Addition to the Reduction Behavior of Cobalt Oxide Particles. *Appl. Catal. A Gen.* **2007**, *333*, 177–191.
(70) van Steen, E.; Sewell, G. S.; Makhothe, R. A.; Micklethwaite, C.; Manstein, H.; de Lange, M.; O'Connor, C. T. TPR Study on the Preparation of Impregnated Co/SiO_2 Catalysts. *J. Catal.* **1996**, *162*, 220–229.
(71) Arnoldy, P.; Moulijn, J. A. Temperature-Programmed Reduction of CoO/Al_2O_3 Catalysts. *J. Catal.* **1985**, *93*, 38–54.
(72) Fischer, N.; Minnermann, M.; Baeumer, M.; van Steen, E.; Claeys, M. Metal Support Interactions in Co_3O_4/Al_2O_3 Catalysts Prepared from w/o Microemulsions. *Catal. Letters* **2012**, *142*, 830–837.
(73) Fischer, N.; van Steen, E.; Claeys, M. Preparation of Supported Nano-Sized Cobalt Oxide and Fcc Cobalt Crystallites. *Catal. Today* **2011**, *171*, 174–179.
(74) Tsakoumis, N. E.; Voronov, A.; Rønning, M.; van Beek, W.; Borg, Ø.; Rytter, E.; Holmen, A. Fischer-Tropsch Synthesis: An XAS/XRPD Combined in Situ Study from Catalyst Activation to Deactivation. *J. Catal.* **2012**, *291*, 138–148.
(75) Kiss, G.; Kliewer, C. E.; DeMartin, G. J.; Culross, C. C.; Baumgartner, J. E. Hydrothermal Deactivation of Silica-Supported Cobalt Catalysts in Fischer-Tropsch Synthesis. *J. Catal.* **2003**, *217*, 127–140.
(76) Moen, A.; Nicholson, D. G.; Clausen, B. S.; Hansen, P. L.; Molenbroek, A.; Steffensen, G. X-Ray Absorption Spectroscopic Studies at the Cobalt K-Edge on a Reduced Al_2O_3-Supported Rhenium-Promoted Cobalt Fischer-Tropsch Catalyst. *Chem. Mater.* **1997**, *9*, 1241–1247.
(77) Farges, F.; Brown, G.; Rehr, J. Ti K-Edge XANES Studies of Ti Coordination and Disorder in Oxide Compounds: Comparison between Theory and Experiment. *Phys. Rev. B* **1997**, *56*, 1809–1819.
(78) Bungmek, W.; Viravathana, P.; Prangsri-aroon, S.; Chotiwan, S.; Deutschmann, O.; Schulz, H. XAS Studies on Promoted and Un-Promoted Silica Supported Cobalt Catalysts for Fischer-Tropsch Synthesis. *Proc. Int. Conf. Environ. Ind. Innov.* **2011**, *12*, 65–69.
(79) Li, C.; Han, X.; Cheng, F.; Hu, Y.; Chen, C.; Chen, J. Phase and Composition Controllable Synthesis of Cobalt Manganese Spinel Nanoparticles towards Efficient Oxygen Electrocatalysis. *Nat. Commun.* **2015**, *6*, 7345.
(80) Moen, A.; Nicholson, D. G.; Rønning, M.; Lamble, G. M.; Lee, J.-F.; Emerich, H. X-Ray Absorption Spectroscopic Study at the Cobalt K-Edge on the Calcination and Reduction of the Microporous Cobalt Silicoaluminophosphate Catalyst CoSAPO-34. *J. Chem. Soc. Faraday Trans.* **1997**, *93*, 4071–4077.
(81) Sirijaruphan, A.; Horváth, A.; Goodwin Jr., J. G.; Oukaci, R. Cobalt Aluminate Formation in Alumina-Supported Cobalt Catalysts: Effects of Cobalt Reduction State and Water Vapor. *Catal. Letters* **2003**, *91*, 89–94.
(82) Tavasoli, A.; Sadagiani, K.; Khorashe, F.; Seifkordi, A. A.; Rohani, A. A.; Nakhaeipour, A. Cobalt Supported on Carbon Nanotubes -- A Promising Novel Fischer-Tropsch Synthesis Catalyst. *Fuel Process. Technol.* **2008**, *89*, 491–498.